

Superfluidity and excitations at unitarity

Dean Lee

Department of Physics, North Carolina State University, Raleigh, NC 27695

Abstract

We present lattice results for spin-1/2 fermions at unitarity, where the effective range of the interaction is zero and the scattering length is infinite. We measure the spatial coherence of difermion pairs for a system of 6, 10, 14, 18, 22, 26 particles with equal numbers of up and down spins in a periodic cube. Using Euclidean time projection, we analyze ground state properties and transient behavior due to low-energy excitations. At asymptotically large values of t we see long-range order consistent with spontaneously broken $U(1)$ fermion-number symmetry and a superfluid ground state. At intermediate times we see exponential decay in the t -dependent signal due to an unknown low-energy excitation. We probe this low-energy excitation further by calculating two-particle correlation functions. We find that the excitation has the properties of a chain of particles extending across the periodic lattice.

Contents

I. Introduction	2
II. Off-diagonal long-range order	4
III. Measured observables in continuum notation	5
IV. Lattice formalism	6
V. Transfer matrix projection method	9
VI. Lattice parameters and error estimates	13
VII. Numerical crosschecks	14
VIII. Results for the renormalization constant Γ	16
IX. Results for the t -dependent profile of G_{ψ^2}	19
X. Results for the lowest excitation energy	21
XI. Two-particle correlations	30
XII. Results for $\rho_{\uparrow\downarrow}$ and $\rho_{\downarrow\downarrow}$	31
XIII. Summary and discussion	35
XIV. Acknowledgements	38
References	38

I. INTRODUCTION

The unitary limit describes a many-body system of nonrelativistic spin-1/2 fermions with zero-range attraction and infinite scattering length. While the unitary limit has a well-defined continuum limit and strong interactions, at zero temperature it has no intrinsic physical scale other than the interparticle spacing. This implies for example at zero tem-

perature the energy per particle and pairing gap are both given by the Fermi energy times a dimensionless constant.

The universal nature of the unitary limit endows it relevance to several areas of physics and the subject has received much recent interest. The ground state is believed to be superfluid with properties somewhere between a Bardeen-Cooper-Schrieffer (BCS) fermionic superfluid at weak coupling and a Bose-Einstein condensate (BEC) of bound dimers at strong coupling [1, 2, 3]. In solid state physics it has been suggested that the crossover from BCS fermionic superfluid to BEC bosonic superfluid describes the pseudogap phase in high-temperature cuprate superconductors [4]. In atomic physics BCS-BEC crossover has been studied extensively with trapped ultracold ${}^6\text{Li}$ and ${}^{40}\text{K}$ atoms. The atoms are sufficiently far apart that the effective range of the interaction is negligible while the scattering length can be adjusted using a magnetic-field Feshbach resonance [5, 6, 7, 8]. In nuclear physics the unitary limit is relevant to the properties of cold dilute neutron matter. The neutron scattering length is about -18 fm while the effective range is 2.8 fm. Therefore the unitary limit is approximately realized when the interparticle spacing is about 10 fm, roughly 0.5% of normal nuclear matter density. Superfluid neutrons at around this density may be present in the inner crust of neutron stars [9, 10].

In this study we measure the low-energy states of unpolarized spin-1/2 fermions in the unitary limit. We use the same lattice projection technique used in [11] to measure the ground state energy. We start with a quantum state with the desired quantum numbers and use the Euclidean time projection operator e^{-Ht} to filter out high-energy excitations. We work with finite systems where the energy spectrum is discrete. Therefore we don't have gapless modes which appear only in the thermodynamic limit. After this filtering we measure spatial correlations of the superfluid order parameter as a function of the projection time t . At asymptotically large values of t we see long-range order consistent with spontaneously broken $U(1)$ fermion-number symmetry and a superfluid ground state. At intermediate times we see exponential decay in the t -dependent signal due to an unknown low-energy excitation. We probe this low-energy excitation further by calculating two-particle correlation functions. We find that the excitation is consistent with a quasi-1D subsystem of particles extending across the periodic lattice.

II. OFF-DIAGONAL LONG-RANGE ORDER

Written in continuum notation the Hamiltonian for the unitary limit is

$$H = -\frac{1}{2m} \sum_{i=\uparrow,\downarrow} \int d^3\vec{r} a_i^\dagger(\vec{r}) \vec{\nabla}^2 a_i(\vec{r}) + C \int d^3\vec{r} a_\downarrow^\dagger(\vec{r}) a_\uparrow^\dagger(\vec{r}) a_\uparrow(\vec{r}) a_\downarrow(\vec{r}). \quad (1)$$

a_i and a_i^\dagger are annihilation and creation operators for fermions with spin i . The mass of the fermion is m , and the coefficient C is cutoff dependent. We discuss later how in lattice regularization C is tuned to make the s-wave scattering length infinite.

The unitary limit Hamiltonian has a global $U(1)$ fermion-number symmetry

$$\begin{bmatrix} a_\uparrow(\vec{r}) \\ a_\downarrow(\vec{r}) \end{bmatrix} \rightarrow e^{i\phi} \begin{bmatrix} a_\uparrow(\vec{r}) \\ a_\downarrow(\vec{r}) \end{bmatrix}, \quad (2)$$

where ϕ is any real constant. It also has a global $SU(2)$ spin symmetry

$$\begin{bmatrix} a_\uparrow(\vec{r}) \\ a_\downarrow(\vec{r}) \end{bmatrix} \rightarrow e^{i\vec{\phi}\cdot\vec{\sigma}} \begin{bmatrix} a_\uparrow(\vec{r}) \\ a_\downarrow(\vec{r}) \end{bmatrix}, \quad (3)$$

where $\vec{\sigma}$ denotes the 2×2 Pauli spin matrices and $\vec{\phi}$ is any real constant three-component vector. Since there is no coupling between intrinsic spin and orbital angular momentum, this $SU(2)$ symmetry should be regarded as an internal symmetry decoupled from spatial rotations.

The lowest-dimensional local bosonic operator that can be constructed from the annihilation field operators is

$$\psi^2(\vec{r}) = a_\uparrow(\vec{r}) a_\downarrow(\vec{r}). \quad (4)$$

We note that ψ^2 is invariant under the $SU(2)$ spin symmetry but phase rotates under the $U(1)$ fermion-number symmetry,

$$\psi^2(\vec{r}) \rightarrow e^{2i\phi} \psi^2(\vec{r}). \quad (5)$$

Therefore if there is some critical temperature below which ψ^2 has long-range spatial correlations,

$$\lim_{|\vec{r}'| \rightarrow \infty} \langle \psi^{2\dagger}(\vec{r}') \psi^2(\vec{0}) \rangle \neq 0, \quad (6)$$

then the $U(1)$ fermion-number symmetry is spontaneously broken. While there are many different ways to characterize superfluid behavior, this condition of off-diagonal long-range order [12, 13] is usually regarded as the standard definition for superfluidity.

III. MEASURED OBSERVABLES IN CONTINUUM NOTATION

In order to highlight the physics content of the lattice calculation we summarize the measured observables in continuum notation. We refer to a state with N_\uparrow up-spin fermions and N_\downarrow down-spin fermions as an N_\uparrow, N_\downarrow state. We also specify the total momentum \vec{P} and total spin S of the $SU(2)$ spin representation. Let $|\Psi_0^{\text{free}}\rangle$ be the free Fermi ground state for the N, N system with $\vec{P} = \vec{0}$ and $S = 0$. We filter out high-energy states using the Euclidean-time projection operator e^{-Ht} ,

$$|\Psi(t)\rangle = e^{-Ht} |\Psi_0^{\text{free}}\rangle. \quad (7)$$

With the projected states $|\Psi(t)\rangle$ we measure the correlation function $G_{\psi^2}(\vec{r}, t_1, t_2)$,

$$G_{\psi^2}(\vec{r}, t_1, t_2) = \frac{1}{\Gamma} \frac{\langle \Psi(t_1) | \psi^{2\dagger}(\vec{r}) \psi^2(\vec{0}) | \Psi(t_2) \rangle}{\langle \Psi(t_1) | \Psi(t_2) \rangle}, \quad (8)$$

where Γ is a renormalization coefficient set by the condition

$$\lim_{t_1, t_2 \rightarrow \infty} G_{\psi^2}(\vec{0}, t_1, t_2) = 1. \quad (9)$$

We consider only finite systems where the energy spectrum is discrete. For large t we have the asymptotic form

$$|\Psi(t)\rangle = c_0 e^{-E_0 t} |\Psi_0\rangle + c_1 e^{-E_1 t} |\Psi_1\rangle + \dots. \quad (10)$$

$|\Psi_0\rangle$ is the normalized ground state with energy E_0 , and $|\Psi_1\rangle$ is the normalized first excited state with energy E_1 . We anticipate the possibility of degeneracy in the low-energy spectrum corresponding with two-particle excitations with momenta \vec{k} and $-\vec{k}$. Since we use a periodic cube with lattice regularization, quantum states in the same irreducible representation of the cubic lattice symmetry group $SO(3, \mathbb{Z})$ are exactly degenerate in energy. But there might also be approximately degenerate excited states whose energy differences are not adequately resolved by the finite values of t measured. We use the notation $|\Psi_{1,i}\rangle$ for the complete set of normalized degenerate excited states with energy E_1 . Using the asymptotic form (10) we get

$$\begin{aligned} G_{\psi^2}(\vec{r}, t_1, t_2) &= A_{00}(\vec{r}) + A_{01}(\vec{r}) e^{-(E_1 - E_0)t_2} + A_{10}(\vec{r}) e^{-(E_1 - E_0)t_1} \\ &+ A_{11}(\vec{r}) e^{-(E_1 - E_0)(t_1 + t_2)} + \dots \end{aligned} \quad (11)$$

where

$$A_{00}(\vec{r}) = \frac{1}{\Gamma} \langle \Psi_0 | \psi^{2\dagger}(\vec{r}) \psi^2(\vec{0}) | \Psi_0 \rangle, \quad (12)$$

$$A_{01}(\vec{r}) = \frac{1}{\Gamma} \sum_i \frac{c_0^* c_{1,i}}{|c_0|^2} \langle \Psi_0 | \psi^{2\dagger}(\vec{r}) \psi^2(\vec{0}) | \Psi_{1,i} \rangle, \quad (13)$$

$$A_{10}(\vec{r}) = \frac{1}{\Gamma} \sum_i \frac{c_{1,i}^* c_0}{|c_0|^2} \langle \Psi_{1,i} | \psi^{2\dagger}(\vec{r}) \psi^2(\vec{0}) | \Psi_0 \rangle, \quad (14)$$

$$A_{11}(\vec{r}) = \frac{1}{\Gamma} \sum_{i,i'} \frac{c_{1,i}^* c_{1,i'}}{|c_0|^2} \langle \Psi_{1,i} | \psi^{2\dagger}(\vec{r}) \psi^2(\vec{0}) | \Psi_{1,i'} \rangle - \frac{1}{\Gamma} \sum_i \frac{|c_{1,i}|^2}{|c_0|^2} \langle \Psi_0 | \psi^{2\dagger}(\vec{r}) \psi^2(\vec{0}) | \Psi_0 \rangle. \quad (15)$$

From the definition of Γ it follows that $A_{00}(\vec{0}) = 1$. In order to determine whether the strongest transient signal comes from $A_{01}(\vec{r})$ and $A_{10}(\vec{r})$ or $A_{11}(\vec{r})$ we will calculate $G_{\psi^2}(\vec{r}, t_1, t_2)$ for two different large time combinations. In one case we let $t_1 = t_2$ and send both to infinity. In the other case we let t_2 be large but fixed and take the limit as t_1 goes to infinity. By analyzing the time dependence we extract the energy difference $E_1 - E_0$, and from the spatial dependence we measure the momentum of the particles in $|\Psi_{1,i}\rangle$ which couple to $\psi^{2\dagger}(\vec{r})\psi^2(\vec{0})$.

IV. LATTICE FORMALISM

Throughout our discussion of the lattice calculation we use dimensionless parameters and operators which correspond with physical values multiplied by the appropriate power of the spatial lattice spacing a . When we need to specify quantities in physical units we write the subscript ‘phys’. In our notation the four-component integer vector \vec{n} labels the lattice sites of a $3 + 1$ dimensional lattice with dimensions $L^3 \times L_t$. \vec{n}_s gives the spatial part of \vec{n} , while n_t is the time component. We write $\hat{l}_s = \hat{1}, \hat{2}, \hat{3}$ for the spatial lattice unit vectors and $\hat{0}$ for the temporal lattice unit vector. The temporal lattice spacing is given by a_t , and $\alpha_t = a_t/a$ is the ratio of the temporal to spatial lattice spacing. We also define $h = \alpha_t/(2m)$, where m is the fermion mass in lattice units.

We briefly discuss four different lattice formulations: the transfer matrix formalism with and without auxiliary fields, and the path integral formalism with and without auxiliary fields. While in the main calculation we use only the transfer matrix formalism with auxiliary fields, the other formulations are useful to provide numerical checks of the simulation data. The four formulations agree exactly even for nonzero spatial and temporal lattice spacings.

The first formulation we consider is the path integral formalism with auxiliary fields. This has been used in varying forms in several grand canonical mean field calculations and lattice simulations at nonzero temperature [14, 15, 16, 17, 18, 19, 20]. We let $c_i(\vec{n})$ and $c_i^*(\vec{n})$ be anticommuting Grassmann fields for spin i , and $s(\vec{n})$ be an auxiliary Hubbard-Stratonovich field. Let \mathcal{Z} be the partition function

$$\mathcal{Z} \propto \int Ds Dc Dc^* \exp[-S(s, c, c^*)], \quad (16)$$

where

$$Ds = \prod_{\vec{n}} ds(\vec{n}), \quad (17)$$

$$Dc Dc^* = \prod_{\vec{n}, i} dc_i(\vec{n}) dc_i^*(\vec{n}). \quad (18)$$

We take as our standard lattice path integral action

$$\begin{aligned} S(s, c, c^*) = & \sum_{\vec{n}, i} \left[c_i^*(\vec{n}) c_i(\vec{n} + \hat{0}) - e^{\sqrt{-C\alpha_t} s(\vec{n}) + \frac{C\alpha_t}{2}} (1 - 6h) c_i^*(\vec{n}) c_i(\vec{n}) \right] \\ & - h \sum_{\vec{n}, l_s, i} \left[c_i^*(\vec{n}) c_i(\vec{n} + \hat{l}_s) + c_i^*(\vec{n}) c_i(\vec{n} - \hat{l}_s) \right] + \frac{1}{2} \sum_{\vec{n}} [s(\vec{n})]^2. \end{aligned} \quad (19)$$

If we include a chemical potential then the action becomes

$$\begin{aligned} S(s, c, c^*) = & \sum_{\vec{n}, i} \left[c_i^*(\vec{n}) c_i(\vec{n} + \hat{0}) - e^{\sqrt{-C\alpha_t} s(\vec{n}) + \frac{C\alpha_t}{2}} e^{\mu\alpha_t} (1 - 6h) c_i^*(\vec{n}) c_i(\vec{n}) \right] \\ & - h e^{\mu\alpha_t} \sum_{\vec{n}, l_s, i} \left[c_i^*(\vec{n}) c_i(\vec{n} + \hat{l}_s) + c_i^*(\vec{n}) c_i(\vec{n} - \hat{l}_s) \right] + \frac{1}{2} \sum_{\vec{n}} [s(\vec{n})]^2. \end{aligned} \quad (20)$$

From this point on it is easy to follow how the chemical potential enters into the other formulations. Therefore we simplify the discussion by setting the chemical potential to zero.

In order to connect the path integral with the transfer matrix formalism, we use the correspondence [21, 22]

$$\begin{aligned} & Tr \left\{ : F_{L_t-1} \left[a_{i'}^\dagger(\vec{n}'_s), a_i(\vec{n}_s) \right] : \times \cdots \times : F_0 \left[a_{i'}^\dagger(\vec{n}'_s), a_i(\vec{n}_s) \right] : \right\} \\ & = \int Dc Dc^* \exp \left\{ \sum_{n_t=0}^{L_t-1} \sum_{\vec{n}_s, i} c_i^*(\vec{n}_s, n_t) [c_i(\vec{n}_s, n_t) - c_i(\vec{n}_s, n_t + 1)] \right\} \\ & \quad \times \prod_{n_t=0}^{L_t-1} F_{n_t} [c_{i'}^*(\vec{n}'_s, n_t), c_i(\vec{n}_s, n_t)] \end{aligned} \quad (21)$$

where $c_i(\vec{n}_s, L_t) = -c_i(\vec{n}_s, 0)$. We use $a_i(\vec{n}_s)$ and $a_i^\dagger(\vec{n}_s)$ to denote the fermion annihilation and creation operators respectively for spin i . The $:$ symbols in the top line of (21) indicate normal ordering. Let us define the transfer matrix operator

$$M_{n_t}(s) \equiv: \exp \left\{ \sum_{\vec{n}_s, i} \left[e^{\sqrt{-C}\alpha_t s(\vec{n}_s, n_t) + \frac{C\alpha_t}{2}} (1 - 6h) - 1 \right] a_i^\dagger(\vec{n}_s) a_i(\vec{n}_s) \right. \\ \left. + h \sum_{\vec{n}_s, l_s, i} \left[a_i^\dagger(\vec{n}_s) a_i(\vec{n}_s + \hat{l}_s) + a_i^\dagger(\vec{n}_s) a_i(\vec{n}_s - \hat{l}_s) \right] \right\} :. \quad (22)$$

We can write the partition function as

$$\mathcal{Z} \propto \int Ds \text{Tr} \{ M_{L_t-1}(s) \times \cdots \times M_0(s) \} \exp \left\{ \frac{1}{2} \sum_{\vec{n}} [s(\vec{n})]^2 \right\}. \quad (23)$$

We now remove the auxiliary field. Integrating over $s(\vec{n})$ in the path integral we obtain [23]

$$\mathcal{Z} \propto \int Dc Dc^* \exp [-S(c, c^*)], \quad (24)$$

$$S(c, c^*) = \sum_{\vec{n}, i} [c_i^*(\vec{n}) c_i(\vec{n} + \hat{0}) - (1 - 6h) c_i^*(\vec{n}) c_i(\vec{n})] \\ - h \sum_{\vec{n}, l_s, i} [c_i^*(\vec{n}) c_i(\vec{n} + \hat{l}_s) + c_i^*(\vec{n}) c_i(\vec{n} - \hat{l}_s)] \\ - (e^{-C\alpha_t} - 1) (1 - 6h)^2 \sum_{\vec{n}} c_{\downarrow}^*(\vec{n}) c_{\uparrow}^*(\vec{n}) c_{\uparrow}(\vec{n}) c_{\downarrow}(\vec{n}). \quad (25)$$

This is probably the simplest formulation for computing Feynman diagrams and the most convenient for setting the lattice interaction coefficient C . As shown in [15] the procedure for setting C involves summing the bubble diagrams shown in FIG. 1, locating the pole in the scattering amplitude, and comparing with Lüscher's formula for energy levels in a finite periodic cube [24, 25],

$$E_{\text{pole}} = \frac{4\pi a_{\text{scatt}}}{mL^3} \left[1 - c_1 \frac{a_{\text{scatt}}}{L} + c_2 \frac{a_{\text{scatt}}^2}{L^2} + \cdots \right], \quad (26)$$

where $c_1 = -2.837297$, $c_2 = 6.375183$. Taking the limit $a_{\text{scatt}} \rightarrow \infty$ we get the interaction coefficient for the unitary limit.

We can use (21) again to derive the corresponding transfer matrix formalism without auxiliary fields,

$$\mathcal{Z} \propto \text{Tr} \{ M_{L_t-1} \times \cdots \times M_0 \}, \quad (27)$$

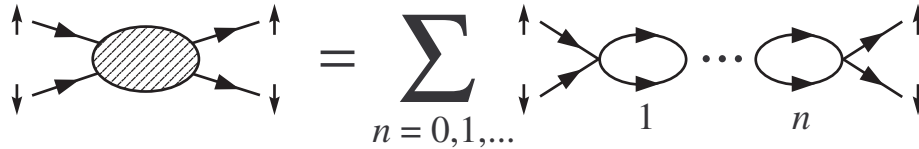


FIG. 1: Two-particle scattering bubble chain diagrams

where

$$M_{n_t} \equiv: \exp \left\{ \begin{aligned} & -6h \sum_{\vec{n}_s, i} a_i^\dagger(\vec{n}_s) a_i(\vec{n}_s) + h \sum_{\vec{n}_s, l_s, i} \left[a_i^\dagger(\vec{n}_s) a_i(\vec{n}_s + \hat{l}_s) + a_i^\dagger(\vec{n}_s) a_i(\vec{n}_s - \hat{l}_s) \right] \\ & + (e^{-C\alpha t} - 1) (1 - 6h)^2 \sum_{\vec{n}_s} a_\downarrow^\dagger(\vec{n}_s) a_\uparrow^\dagger(\vec{n}_s) a_\uparrow(\vec{n}_s) a_\downarrow(\vec{n}_s) \end{aligned} \right\} : . \quad (28)$$

Since there is no time-dependent auxiliary field, M_{n_t} is the same for each time step n_t . This formulation is useful in few-body systems with no sign problem. In [23] it was used to calculate the binding energy of the $SU(4)$ Wigner-symmetric triton.

V. TRANSFER MATRIX PROJECTION METHOD

We use the transfer matrix projection method introduced in [11]. In this paper we consider the values $N = 1, 3, 5, 7, 9, 11, 13$. For each spin we fill the momentum states comprising $|\Psi_0^{\text{free}}\rangle$ in the order shown in Table 1. We observe that for each value of N , $|\Psi_0^{\text{free}}\rangle$ has zero total momentum and zero total spin. For $N = 7$ we have the special case where $|\Psi_0^{\text{free}}\rangle$ is also invariant under $SO(3, \mathbb{Z})$ rotations.

N	additional momenta filled
1	$\langle 0, 0, 0 \rangle$
3	$\langle \frac{2\pi}{L}, 0, 0 \rangle, \langle -\frac{2\pi}{L}, 0, 0 \rangle$
5	$\langle 0, \frac{2\pi}{L}, 0 \rangle, \langle 0, -\frac{2\pi}{L}, 0 \rangle$
7	$\langle 0, 0, \frac{2\pi}{L} \rangle, \langle 0, 0, -\frac{2\pi}{L} \rangle$
9	$\langle \frac{2\pi}{L}, \frac{2\pi}{L}, 0 \rangle, \langle -\frac{2\pi}{L}, -\frac{2\pi}{L}, 0 \rangle$
11	$\langle \frac{2\pi}{L}, -\frac{2\pi}{L}, 0 \rangle, \langle -\frac{2\pi}{L}, \frac{2\pi}{L}, 0 \rangle$
13	$\langle 0, \frac{2\pi}{L}, \frac{2\pi}{L} \rangle, \langle 0, -\frac{2\pi}{L}, -\frac{2\pi}{L} \rangle$

Table 1. Filling sequence of momentum states

Using the auxiliary field transfer matrix defined in (22) we construct

$$|\Psi(t), s\rangle \equiv M_{n_t-1}(s) \times \cdots \times M_0(s) |\Psi_0^{\text{free}}\rangle, \quad (29)$$

where $t = n_t a_t$. This is the analog of

$$|\Psi(t)\rangle = e^{-Ht} |\Psi_0^{\text{free}}\rangle \quad (30)$$

defined above in the continuum notation. We compute spatial correlations of the difermion pair operator $\psi^2(\vec{n}_s) = a_\uparrow(\vec{n}_s)a_\downarrow(\vec{n}_s)$,

$$G_{\psi^2}^{\text{bare}}(\vec{n}_s, t_1, t_2) = \frac{\int Ds \langle \Psi(t_1), s | \psi^{2\dagger}(\vec{n}_s) \psi^2(\vec{0}) | \Psi(t_2), s \rangle \exp \left\{ -\frac{1}{2} \sum_{\vec{n}} [s(\vec{n})]^2 \right\}}{\int Ds \langle \Psi(t_1), s | \Psi(t_2), s \rangle \exp \left\{ -\frac{1}{2} \sum_{\vec{n}} [s(\vec{n})]^2 \right\}}. \quad (31)$$

The inner products in the numerator and denominator are to be defined shortly. We use the superscript ‘bare’ since matrix elements of the composite operators ψ^2 and $\psi^{2\dagger}$ diverge in the continuum limit. We take care of this renormalization by rescaling the correlation function,

$$G_{\psi^2}(\vec{n}_s, t_1, t_2) = \frac{1}{\Gamma} G_{\psi^2}^{\text{bare}}(\vec{n}_s, t_1, t_2), \quad (32)$$

where

$$\Gamma = \lim_{t_1, t_2 \rightarrow \infty} G_{\psi^2}^{\text{bare}}(\vec{0}, t_1, t_2). \quad (33)$$

$M_{n_t}(s)$ consists entirely of single-body operators interacting with the background auxiliary field and has no direct interactions between particles. This may not be obvious from the complicated form for $M_{n_t}(s)$ in (22). To see this more clearly we pretend for the moment that the N up-spin particles and N down-spin particles are all distinguishable. We label the newly distinguishable particles with the label $X = 1, 2, \dots, 2N - 1, 2N$. This error in quantum statistics has no effect on the final answer if the initial and final state wavefunctions are completely antisymmetric in the up-spin and down-spin variables. Since we have exactly one particle of each type X , the normal-ordered operator $M_{n_t}(s)$ can be factorized as a product of terms of the form

$$M_{n_t}(s) = \prod_X M_{n_t}^X(s), \quad (34)$$

where

$$\begin{aligned}
M_{n_t}^X(s) &= 1 + \left[e^{\sqrt{-C\alpha_t s(\vec{n}_s, n_t) + \frac{C\alpha_t}{2}}(1 - 6h) - 1} \sum_{\vec{n}_s} a_X^\dagger(\vec{n}_s) a_X(\vec{n}_s) \right. \\
&\quad \left. + h \sum_{\vec{n}_s, \hat{l}_s} \left[a_X^\dagger(\vec{n}_s) a_X(\vec{n}_s + \hat{l}_s) + a_X^\dagger(\vec{n}_s) a_X(\vec{n}_s - \hat{l}_s) \right] \right]. \tag{35}
\end{aligned}$$

If the particle stays at the same spatial lattice site from time step n_t to $n_t + 1$, then the corresponding matrix element of $M_{n_t}^X(s)$ is

$$e^{\sqrt{-C\alpha_t s(\vec{n}) + \frac{C\alpha_t}{2}}(1 - 6h)}. \tag{36}$$

If the particle hops to a neighboring lattice site from time step n_t to $n_t + 1$ then the corresponding matrix element of $M_{n_t}^X(s)$ is h . All other elements of $M_{n_t}^X(s)$ are zero.

We can therefore compute the full $2N$ -body matrix element as the square of the determinant of the single-particle matrix elements,

$$\begin{aligned}
\langle \Psi(t_1), s | \Psi(t_2), s \rangle &\equiv \langle \Psi_0^{\text{free}} | M_{L_t-1}(s) \times \cdots \times M_0(s) | \Psi_0^{\text{free}} \rangle \\
&= [\det M(s, t_1 + t_2)]^2, \tag{37}
\end{aligned}$$

$$M_{ij}(s, t_1 + t_2) = \langle p_i^X | M_{L_t-1}^X(s) \times \cdots \times M_0^X(s) | p_j^X \rangle, \tag{38}$$

where i, j go from 1 to N and $t_1 + t_2 = L_t a_t$. The states $|p_j^X\rangle$ are the single-particle momentum states for the up spins (or down spins) comprising our Slater determinant initial and final state $|\Psi_0^{\text{free}}\rangle$. The square of the determinant arises from the fact that we have the same transfer matrix elements and the same momentum states $|p_j^X\rangle$ for both up and down spins. Since the square of the determinant is nonnegative, there is no sign problem.

We sample configurations according to the weight

$$\exp \left\{ -\frac{1}{2} \sum_{\vec{n}} [s(\vec{n})]^2 + 2 \ln [|\det M(s, t_1 + t_2)|] \right\}. \tag{39}$$

The updating procedure is done using hybrid Monte Carlo [26]. This involves computing molecular dynamics trajectories for

$$H(s, p) = \frac{1}{2} \sum_{\vec{n}} (p(\vec{n}))^2 + V(s), \tag{40}$$

where $p(\vec{n})$ is the conjugate momentum for $s(\vec{n})$ and

$$V(s) = \frac{1}{2} \sum_{\vec{n}} (s(\vec{n}))^2 - 2 \ln [|\det M(s, t_1 + t_2)|]. \tag{41}$$

More details of the updating procedure are given in [11]. For each configuration we compute the observable

$$O(\vec{n}_s, t_1, t_2, s) = \frac{\langle \Psi(t_1), s | \psi^{2\dagger}(\vec{n}_s) \psi^2(\vec{0}) | \Psi(t_2), s \rangle}{\langle \Psi(t_1), s | \Psi(t_2), s \rangle}. \quad (42)$$

This can be written in terms of the matrix $M(s, t_1 + t_2)$ as we now show.

We start with

$$\begin{aligned} & \langle \Psi(t_1), s | \psi^{2\dagger}(\vec{n}_s) \psi^2(\vec{0}) | \Psi(t_2), s \rangle \\ & \equiv \langle \Psi_0^{\text{free}} | M_{L_{t_1}-1}(s) \times \cdots \times M_{n_{t_2}}(s) \psi^{2\dagger}(\vec{n}_s) \psi^2(\vec{0}) M_{n_{t_2}-1}(s) \times \cdots \times M_0(s) | \Psi_0^{\text{free}} \rangle \end{aligned} \quad (43)$$

where $t_1 + t_2 = L_t a_t$ and $t_2 = n_{t_2} a_t$. For each spin the $\psi^{2\dagger}(\vec{n}_s) \psi^2(\vec{0})$ operator replaces one matrix element from $M(s, t_1 + t_2)$, call it the entry in the k th row and l th column, with the new matrix element

$$g_{kl}(\vec{n}_s, s, t_1, t_2) = \langle p_k^X | M_{L_{t_1}-1}^X(s) \times \cdots \times M_{n_{t_2}}^X(s) a_X^\dagger(\vec{n}_s) a_X(\vec{0}) M_{n_{t_2}-1}^X(s) \times \cdots \times M_0^X(s) | p_l^X \rangle. \quad (44)$$

Instead of the full $N \times N$ matrix determinant $\det M(s, t_1 + t_2)$, in this case we get $g_{kl}(\vec{n}_s, s, t_1, t_2)$ times the entry in the k th row and l th column of the cofactor matrix of $M(s, t_1 + t_2)$. This cofactor matrix element is $(-1)^{k+l}$ times the determinant of the remaining $(N-1) \times (N-1)$ matrix with the k th row and l th column of $M(s, t_1 + t_2)$ deleted, and it can be calculated as

$$\det M(s, t_1 + t_2) \times [M^{-1}(s, t_1 + t_2)]_{lk}, \quad (45)$$

where M^{-1} is the matrix inverse of M . Summing over k and l and squaring the result for the two spins, we get

$$\begin{aligned} & \langle \Psi(t_1), s | \psi^{2\dagger}(\vec{n}_s) \psi^2(\vec{0}) | \Psi(t_2), s \rangle \\ & = \left\{ \det M(s, t_1 + t_2) \times \sum_{k,l} g_{kl}(\vec{n}_s, s, t_1, t_2) [M^{-1}(s, t_1 + t_2)]_{lk} \right\}^2. \end{aligned} \quad (46)$$

Therefore our observable is

$$O(\vec{n}_s, t_1, t_2, s) = \left\{ \sum_{k,l} g_{kl}(\vec{n}_s, s, t_1, t_2) [M^{-1}(s, t_1 + t_2)]_{lk} \right\}^2. \quad (47)$$

By measuring the ensemble average of $O(\vec{n}_s, t_1, t_2, s)$ we get an unbiased estimate of $G_{\psi^2}^{\text{bare}}(\vec{n}_s, t_1, t_2)$.

VI. LATTICE PARAMETERS AND ERROR ESTIMATES

Our choice for the physical values of the fermion mass and lattice spacings are irrelevant to the universal physics of the unitary limit. Nevertheless we must assign values to these parameters, and the values we choose are motivated by the dilute neutron system. We use a fermion mass of 939 MeV and lattice spacings $a = (50 \text{ MeV})^{-1}$, $a_t = (24 \text{ MeV})^{-1}$. For these parameters we find in the unitary limit, $C_{\text{phys}} = -1.203 \times 10^{-4} \text{ MeV}^{-2}$.

For each simulation we compute roughly 2×10^5 hybrid Monte Carlo trajectories, split across four processors running completely independent trajectories. Averages and errors are computed by comparing the results of each processor. We use double precision arithmetic to compute $\det M(s, t_1 + t_2)$ and $O(\vec{n}_s, t_1, t_2, s)$. All systematic errors produced by double precision roundoff error and exceptional configurations are monitored in the following way. We introduce a small positive parameter ϵ and reject any hybrid Monte Carlo trajectories which generate a configuration with

$$|\det M(s, t_1 + t_2)| < \epsilon^N \prod_{i=1, \dots, N} |M_{ii}(s, t_1 + t_2)|. \quad (48)$$

We then take the limit $\epsilon \rightarrow 0^+$ to determine if poorly-conditioned matrices make any detectable contribution to our observables. We consider values for ϵ as small as 10^{-7} . If as we take $\epsilon \rightarrow 0^+$ any systematic error can be detected above the stochastic error level, then we throw out the measurement and do not include it in the final results. The error bars we present are therefore estimates of the total error for each lattice system. There are no additional errors other than the lattice spacing dependence.

In the unitary limit our Euclidean variables t_1 and t_2 can be replaced by the dimensionless combinations $\frac{t_1}{mL^2}$ and $\frac{t_2}{mL^2}$. More convenient though is to use the dimensionless combinations $E_F t_1$ and $E_F t_2$, where E_F is the Fermi energy

$$E_F = \frac{k_F^2}{2m} = \frac{(6\pi^2 N)^{2/3}}{2mL^2} \approx 7.596 \frac{N^{2/3}}{mL^2}. \quad (49)$$

At unitarity we can reach the continuum limit at fixed particle number by increasing L , the length of the periodic cube in lattice units. This may seem an unusual way to take the continuum limit. It works only in scale invariant theories such as the unitary limit or noninteracting fermions where the only physical scale is the interparticle spacing. Since the number of particles is fixed, the spacing between particles as measured in lattice units

increases as we increase L . Therefore $L \rightarrow \infty$ corresponds with the continuum limit. By comparing results for different L we obtain an error estimate for the extrapolation to the continuum limit.

VII. NUMERICAL CROSSCHECKS

To test the lattice codes, we have run simulations for several systems where the final answer can be calculated accurately by alternative means. For the first test we consider the noninteracting fermion system for the 7,7 system with total momentum $\vec{P} = \vec{0}$ and total spin $S = 0$. We take $L = 4$ and set L_t large enough to extract the limit

$$\lim_{t_1, t_2 \rightarrow \infty} G_{\psi^2}^{\text{bare}}(\vec{n}_s, t_1, t_2) \quad (50)$$

for $\vec{n}_s = \langle n_x, 0, 0 \rangle$ with $n_x = 0, 1, 2$. We perform the numerical check using the path integral action $S(c, c^*)$ in (25). For temperature $T = 0.022E_F$ and chemical potential $\mu = 0.97E_F$ we apply the free field Feynman rules for the ψ^2 correlation function. For this chemical potential at such low temperatures we should see 7 up spins and 7 down spins in the ground state with $\vec{P} = \vec{0}$ and $S = 0$. A comparison of the simulation results and the free grand canonical calculations is shown Table 2. We see that the free fermion results agree to six-digit precision.

n_x	Simulation results	Free grand canonical
0	1.19629×10^{-2}	1.19629×10^{-2}
1	6.10352×10^{-3}	6.10352×10^{-3}
2	2.19727×10^{-3}	2.19727×10^{-3}

Table 2. Simulation results and free grand canonical calculations for 7,7

Next we turn on a weak attractive coupling $C_{\text{phys}} = -1.25 \times 10^{-5} \text{ MeV}^{-2}$ for the same 7,7 system with $\vec{P} = \vec{0}$ and $S = 0$. This coupling corresponds with a weak-coupling low-density expansion parameter $k_F a_{\text{scatt}} = -0.043$. Using $T = 0.022E_F$ and $\mu = 0.97E_F$ we use the path integral action $S(c, c^*)$ to compute the free fermion result as well as the $O(k_F a_{\text{scatt}})$ correction to the ψ^2 correlation function. The $O(k_F a_{\text{scatt}})$ term requires summing the two-particle bubble chain shown in FIG. 1. A comparison of the simulation results and

perturbative calculations is shown in Table 3. The $O(k_F^2 a_{\text{scatt}}^2)$ correction should be of size roughly 10^{-4} for $n_x = 0$, 5×10^{-5} for $n_x = 1$, and 2×10^{-5} for $n_x = 2$. We see that the simulation results and perturbative calculations agree within deviations roughly matching the size estimates for the $O(k_F^2 a_{\text{scatt}}^2)$ term.

n_x	Simulation results	Perturbative grand canonical
0	$1.3715(1) \times 10^{-2}$	1.3775×10^{-2}
1	$6.999(2) \times 10^{-3}$	7.0295×10^{-3}
2	$2.536(1) \times 10^{-3}$	2.5476×10^{-3}

Table 3. Simulation results and perturbative grand canonical calculations for 7, 7

To test that the code is running properly at the unitary limit, we perform simulations for the 1, 1 system at $\vec{P} = \vec{0}$ and $S = 0$ at unitarity. We use $L = 4$ and compute $G_{\psi^2}^{\text{bare}}(\vec{n}_s, t_1, t_2)$. We take $\vec{n}_s = \langle n_x, 0, 0 \rangle$ for $n_x = 0, 1, 2$ and various numbers of time steps $n_{t_1} = n_{t_2}$. Since there are only two particles with zero total momentum there should be no dependence on the spatial coordinate n_x . For the numerical check we use M_{n_t} , the transfer matrix without auxiliary fields defined in (28), to compute the exact two-body transfer matrix in the rest frame. The results for the lattice simulation and the exact two-body calculation are shown in Table 4. We see that the simulation results agree with the exact results up to errors the size of the estimated stochastic noise.

n_x	$n_{t_1} = n_{t_2} = 2$	$n_{t_1} = n_{t_2} = 4$	$n_{t_1} = n_{t_2} = 6$
0	$6.946(9) \times 10^{-4}$	$1.156(4) \times 10^{-3}$	$1.564(4) \times 10^{-3}$
1	$6.88(3) \times 10^{-4}$	$1.19(4) \times 10^{-3}$	$1.58(6) \times 10^{-3}$
2	$6.92(1) \times 10^{-4}$	$1.147(6) \times 10^{-3}$	$1.53(3) \times 10^{-3}$
Exact	6.948×10^{-4}	1.153×10^{-3}	1.573×10^{-3}

Table 4: Simulation results and exact two-body calculation for 1, 1 at unitarity

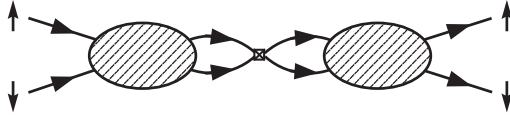


FIG. 2: One insertion of the operator $a_{\downarrow}^{\dagger}(\vec{r})a_{\uparrow}^{\dagger}(\vec{r})a_{\uparrow}(\vec{r})a_{\downarrow}(\vec{r})$

VIII. RESULTS FOR THE RENORMALIZATION CONSTANT Γ

Throughout we consider systems with total momentum $\vec{P} = \vec{0}$ and total spin $S = 0$. The renormalization constant Γ for the N, N system is given by

$$\Gamma = \lim_{t_1, t_2 \rightarrow \infty} G_{\psi^2}^{\text{bare}}(\vec{0}, t_1, t_2) = \langle \Psi_0 | a_{\downarrow}^{\dagger}(\vec{0})a_{\uparrow}^{\dagger}(\vec{0})a_{\uparrow}(\vec{0})a_{\downarrow}(\vec{0}) | \Psi_0 \rangle \quad (51)$$

where $|\Psi_0\rangle$ is the normalized ground state. Γ gives the probability that a given lattice site has both an up-spin and down-spin particle. As shown in FIG. 2, one insertion of the operator $a_{\downarrow}^{\dagger}(\vec{r})a_{\uparrow}^{\dagger}(\vec{r})a_{\uparrow}(\vec{r})a_{\downarrow}(\vec{r})$ produces two extra fermion bubbles. In the continuum limit each of these bubbles are proportional to the inverse lattice spacing a^{-1} plus momentum-dependent terms which are finite as $a \rightarrow 0$. Therefore in the continuum limit Γ_{phys} is proportional to a^{-2} plus subleading terms proportional to a^{-1} .

The coefficient of a^{-2} in Γ_{phys} contains some useful information about physics near the unitarity point. We note that

$$\Gamma = \langle \Psi_0 | a_{\downarrow}^{\dagger}(\vec{0})a_{\uparrow}^{\dagger}(\vec{0})a_{\uparrow}(\vec{0})a_{\downarrow}(\vec{0}) | \Psi_0 \rangle \approx -\frac{1}{\alpha_t L^3} \frac{d}{dC'} \langle \Psi_0 | M_{nt} | \Psi_0 \rangle, \quad (52)$$

where M_{nt} is the transfer matrix without auxiliary fields defined in (28), and

$$C' = -\frac{(e^{-C\alpha_t} - 1)(1 - 6h)^2}{\alpha_t}. \quad (53)$$

We have dropped terms which are $O(a_t)$ and vanish as the temporal lattice spacing goes to zero. If E_0 is the ground state energy then

$$\langle \Psi_0 | M_{nt} | \Psi_0 \rangle = e^{-E_0\alpha_t}, \quad (54)$$

$$\Gamma \approx -\frac{1}{\alpha_t L^3} \frac{d}{dC'} e^{-E_0\alpha_t} \approx \frac{1}{L^3} \frac{dE_0}{dC'}. \quad (55)$$

Let us parameterize the ground state energy per particle near the unitary limit as an expansion in $k_F^{-1} a_{\text{scatt}}^{-1}$,

$$\frac{E_0}{N+N} = \frac{3}{5} \frac{k_F^2}{2m} [\xi - \xi_1 k_F^{-1} a_{\text{scatt}}^{-1} + O(k_F^{-2} a_{\text{scatt}}^{-2})]. \quad (56)$$

The renormalization condition relating C' and a_{scatt} gives [15]

$$\frac{d}{da_{\text{scatt}}^{-1}} = \frac{m}{4\pi} \frac{d}{dC'^{-1}} = -\frac{mC'^2}{4\pi} \frac{d}{dC'}. \quad (57)$$

Using

$$k_F = \frac{(6\pi^2 N)^{1/3}}{L}, \quad (58)$$

and combining (55), (56), (57) we find

$$\xi_1 = -\frac{5m}{3Nk_F} \frac{dE_0}{da_{\text{scatt}}^{-1}} = \frac{5m^2 C'^2 L^4}{12\pi (6\pi^2)^{1/3} N^{4/3}} \Gamma. \quad (59)$$

Since C'_{phys} is proportional to the lattice spacing a , we deduce that the leading divergence of Γ_{phys} is proportional to a^{-2} as predicted before. This anomalous dimensional scaling can also be seen from the L^{-4} dependence of Γ rather than the naive L^{-6} scaling expected for an operator which is the square of a local density.

We determine Γ by fitting $G_{\psi^2}^{\text{bare}}(\vec{0}, t/2, t/2)$ at large $E_F t$ to the asymptotic form

$$G_{\psi^2}^{\text{bare}}(\vec{0}, t/2, t/2) \approx \Gamma - b e^{-\eta E_F t}. \quad (60)$$

The value of Γ is then used to determine ξ_1 . We show the results for $N = 3, 5, 7, 9, 11, 13$ and $L = 4, 5, 6$ in Table 5. We have extrapolated linearly in L^{-1} as $L \rightarrow \infty$ to remove the subleading a^{-1} dependence in $G_{\psi^2}^{\text{bare}}(\vec{0}, t/2, t/2)$. If there are no significant changes for $N > 13$ we estimate that in the limit $N \rightarrow \infty$, $\xi_1 = 1.0(1)$.

L	3, 3	5, 5	7, 7	9, 9	11, 11	13, 13
4	0.696(2)	0.647(2)	0.597(2)	0.595(2)	—	—
5	0.77(1)	0.719(5)	0.662(3)	0.661(2)	0.652(2)	0.639(2)
6	0.84(3)	0.785(4)	0.69(1)	0.711(4)	0.71(1)	0.70(1)
∞	1.08(4)	1.05(4)	0.91(4)	0.93(4)	1.00(5)	1.01(5)

Table 5: Results for ξ_1

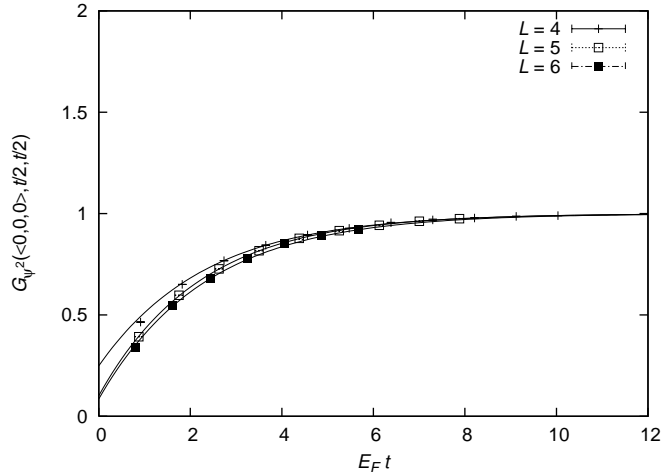


FIG. 3: A comparison of $G_{\psi^2}(\vec{0}, t/2, t/2)$ and the asymptotic fit $1 - \frac{b}{\Gamma} e^{-\eta E_F t}$ for the 9,9 system with $L = 4, 5, 6$.

In FIG. 3 we show a comparison of the renormalized correlation function

$$G_{\psi^2}(\vec{0}, t/2, t/2) = \frac{1}{\Gamma} G_{\psi^2}^{\text{bare}}(\vec{0}, t/2, t/2) \quad (61)$$

and the asymptotic fit

$$1 - \frac{b}{\Gamma} e^{-\eta E_F t} \quad (62)$$

for the 9,9 system and $L = 4, 5, 6$. In the unitary limit we expect agreement for different values of L when plotted as functions of $E_F t$, and this appear to be the case.

The energy $\eta \cdot E_F$ characterizing the exponential decay of the transient signal in $G_{\psi^2}(\vec{0}, t/2, t/2)$ is similar to the energy $\delta \cdot E_F$ measured in the function $\xi_{N,N}(t)$ described in [11]. This might perhaps be a threshold for a certain type of excitation or a maximum in the overlap of $|\Psi_0^{\text{free}}\rangle$ with the spectral density projection operator. The answer is not clear. In the next section we find another excitation with the same quantum numbers but much lower energy. This suggests that our fit with only one exponential time constant may not be a reliable method to determine the higher excitation energy, and a multistate analysis should be used. The interpretation of the apparent energy scale $\eta \cdot E_F$ will require further study.

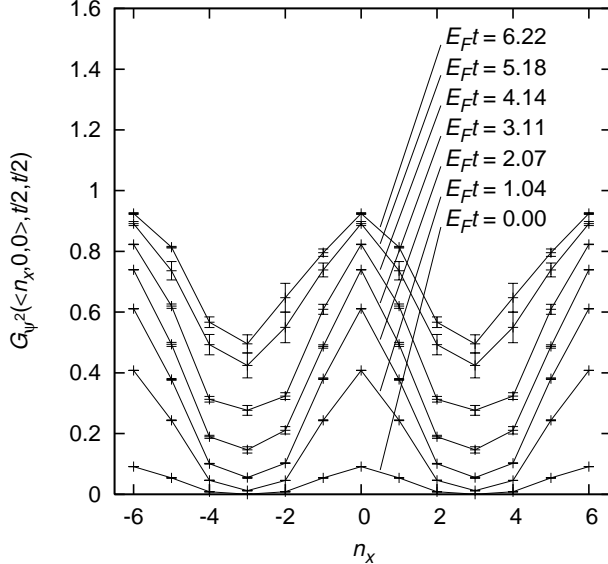


FIG. 4: The renormalized correlation function $G_{\psi^2}(\vec{n}_s, t/2, t/2)$ for the 13,13 system with $L = 6$, $\vec{n}_s = \langle n_x, 0, 0 \rangle$, and $E_F t$ between 0 and 6.22.

IX. RESULTS FOR THE t -DEPENDENT PROFILE OF G_{ψ^2}

We study the dependence of G_{ψ^2} on the spatial separation \vec{n}_s and Euclidean projection time t . In all cases we consider systems with total momentum $\vec{P} = \vec{0}$ and total spin $S = 0$. In FIG. 4 we show the renormalized correlation function $G_{\psi^2}(\vec{n}_s, t/2, t/2)$ for the 13,13 system at unitarity with $L = 6$, $\vec{n}_s = \langle n_x, 0, 0 \rangle$, and $E_F t$ between 0 and 6.22. In order to make the periodicity of the lattice visually clear we show two full lattice lengths.

There are several features in this plot which indicate some interesting physics. First of all ψ^2 appears to have long-range order. With a total of 26 particles we cannot probe distances far beyond k_F^{-1} . But for large $E_F t$ we do find that $G_{\psi^2}(\vec{n}_s, t/2, t/2)$ averaged over the entire lattice is greater than 0.5. We recall $G_{\psi^2}(\vec{n}_s, t/2, t/2)$ is normalized so that the peak value at $\vec{n}_s = \vec{0}$ is 1 as $E_F t \rightarrow \infty$. The second point of interest is that for $\vec{n}_s \neq \vec{0}$ the transient signal has a very long time constant. This long constant time is not apparent at $\vec{n}_s = \vec{0}$. There the transient signal has a shorter time constant, $(\eta \cdot E_F)^{-1}$ in the notation of the previous section. The slow transient signal corresponds with a much lower energy scale and appears to have an approximate $\cos(2\pi n_x/L) - 1$ spatial dependence.

The time constant is easier to see if we plot $G_{\psi^2}(\vec{n}_s, t/2, t/2)$ as a function of $E_F t$. In

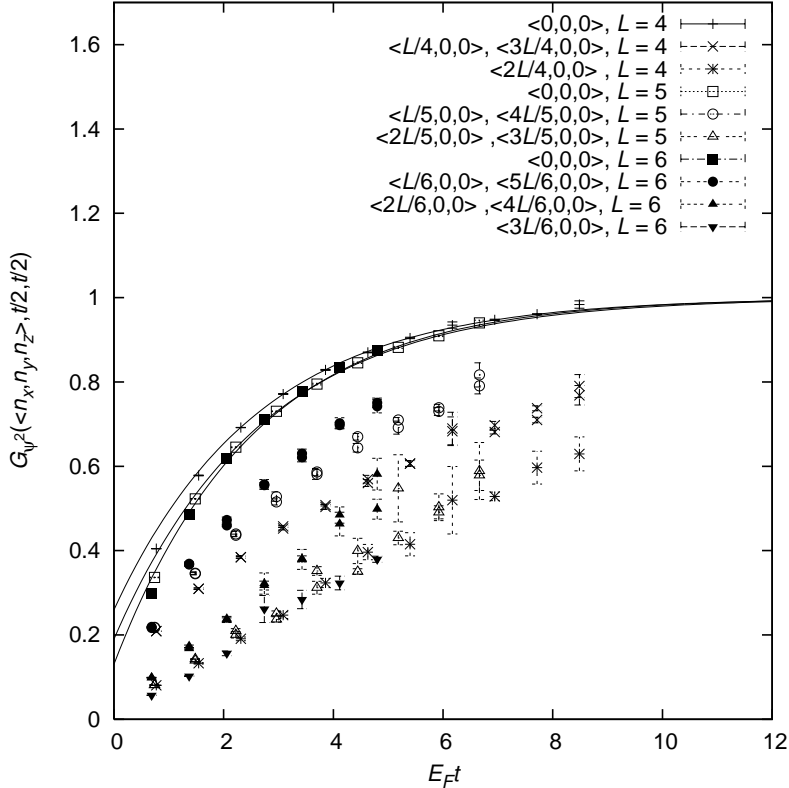


FIG. 5: The renormalized correlation function $G_{\psi^2}(\vec{n}_s, t/2, t/2)$ versus $E_F t$ for the 7, 7 system with $L = 4, 5, 6$ and $\vec{n}_s = \langle n_x, 0, 0 \rangle$. For visual clarity datapoints with errorbars exceeding 0.1 are not shown.

FIG. 5 we show the renormalized correlation function $G_{\psi^2}(\vec{n}_s, t/2, t/2)$ versus $E_F t$ for the 7, 7 system with $L = 4, 5, 6$ and $\vec{n}_s = \langle n_x, 0, 0 \rangle$. We can see quite clearly the fast exponential tail of the transient signal for $\vec{n}_s = \vec{0}$ and the slow exponential tail for $\vec{n}_s \neq \vec{0}$. In the unitary limit, $G_{\psi^2}(\vec{n}_s, t/2, t/2)$ as a function of $E_F t$ for different L should agree for the same ratio \vec{n}_s/L . The data in FIG. 5 shows quite clearly this unitary limit scaling.

In FIG. 6 the renormalized correlation function $G_{\psi^2}(\vec{n}_s, t/2, t/2)$ is shown for the 5, 5 system with $L = 4, 5, 6$ and $\vec{n}_s = \langle n_x, 0, 0 \rangle$. We again see the fast exponential tail of the transient signal at $\vec{n}_s = \vec{0}$ and the slow exponential tail for $\vec{n}_s \neq \vec{0}$. There is good agreement for different values of L with the same \vec{n}_s/L .

In FIG. 7 $G_{\psi^2}(\vec{n}_s, t/2, t/2)$ is shown for the same 5, 5 system with $L = 4, 5, 6$, but this time along the z -axis, $\vec{n}_s = \langle 0, 0, n_z \rangle$. In this case the long time constant previously seen for $\vec{n}_s \neq \vec{0}$ is no longer visible. The distinction between the x - and z -axes can be

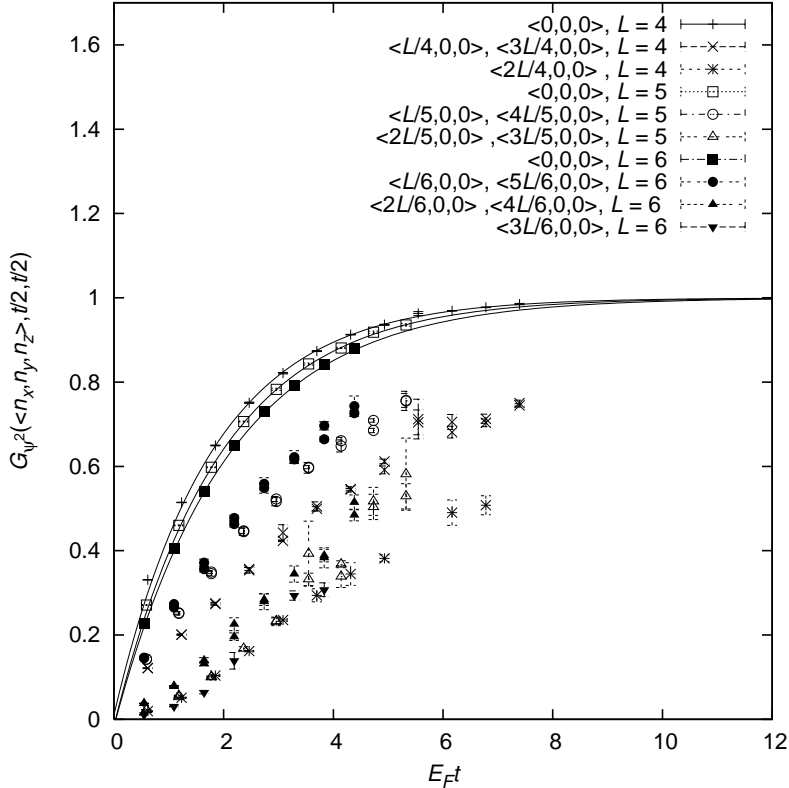


FIG. 6: The renormalized correlation function $G_{\psi^2}(\vec{n}_s, t/2, t/2)$ versus $E_F t$ for the 5, 5 system with $L = 4, 5, 6$ and $\vec{n}_s = \langle n_x, 0, 0 \rangle$. For visual clarity datapoints with errorbars exceeding 0.1 are not shown.

explained by the non- $SO(3, \mathbb{Z})$ invariant momentum filling for $|\Psi_0^{\text{free}}\rangle$. As shown in Table 1, $|\Psi_0^{\text{free}}\rangle$ contains the momentum states $\langle \frac{2\pi}{L}, 0, 0 \rangle$ and $\langle -\frac{2\pi}{L}, 0, 0 \rangle$ but not the momentum states $\langle 0, 0, \frac{2\pi}{L} \rangle$ and $\langle 0, 0, -\frac{2\pi}{L} \rangle$. This produces an overlap with some low-energy excitation with an approximate $\cos(2\pi n_x/L) - 1$ profile in $G_{\psi^2}(\vec{n}_s, t/2, t/2)$ but a much weaker overlap if the same excitation is aligned along the z -axis.

X. RESULTS FOR THE LOWEST EXCITATION ENERGY

We now measure the energy of the lowest excitation. We first construct combinations of $G_{\psi^2}(\vec{n}_s, t_1, t_2)$ which maximize the signal to noise ratio. For $N = 3$ the low-energy excitation does not couple strongly to $G_{\psi^2}(\vec{n}_s, t_1, t_2)$ for \vec{n}_s along the y - and z -axes. Therefore we use

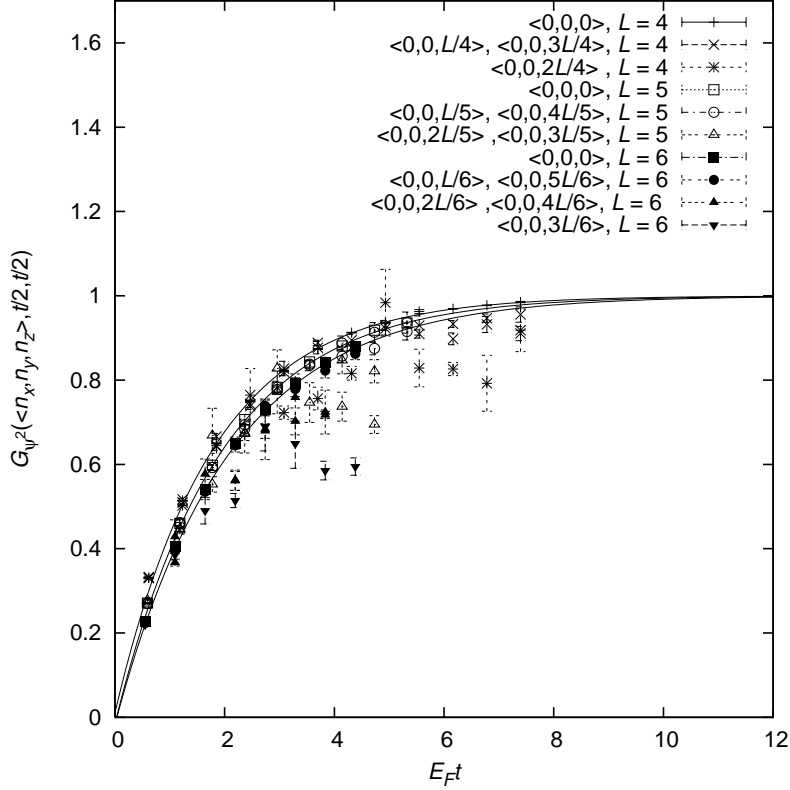


FIG. 7: The renormalized correlation function $G_{\psi^2}(\vec{n}_s, t/2, t/2)$ versus $E_F t$ for the 5, 5 system with $L = 4, 5, 6$ and $\vec{n}_s = \langle 0, 0, n_z \rangle$. For visual clarity datapoints with errorbars exceeding 0.1 are not shown.

only data along the x -axis. We define

$$\begin{aligned} & \delta_x^2 G_{\psi^2}(t_1, t_2) \\ &= L^2 \left\{ G_{\psi^2}(\vec{0}, t_1, t_2) - \frac{1}{2} [G_{\psi^2}(\langle 1, 0, 0 \rangle, t_1, t_2) + G_{\psi^2}(\langle -1, 0, 0 \rangle, t_1, t_2)] \right\}. \end{aligned} \quad (63)$$

For $N = 5$ the coupling is weak only along the z -axis and so we define

$$\begin{aligned} & \delta_{xy}^2 G_{\psi^2}(t_1, t_2) \\ &= L^2 \left\{ G_{\psi^2}(\vec{0}, t_1, t_2) - \frac{1}{4} \left[\begin{aligned} & G_{\psi^2}(\langle 1, 0, 0 \rangle, t_1, t_2) + G_{\psi^2}(\langle -1, 0, 0 \rangle, t_1, t_2) \\ & + G_{\psi^2}(\langle 0, 1, 0 \rangle, t_1, t_2) + G_{\psi^2}(\langle 0, -1, 0 \rangle, t_1, t_2) \end{aligned} \right] \right\}. \end{aligned} \quad (64)$$

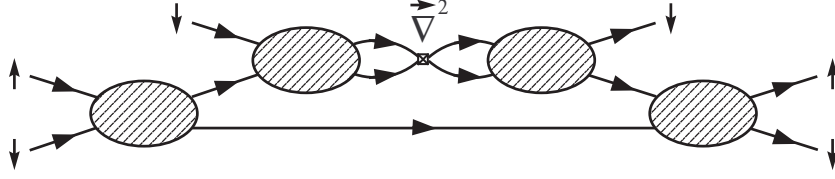


FIG. 8: One insertion of the operator $\frac{1}{\Gamma} a_{\downarrow}^{\dagger}(\vec{r}) a_{\uparrow}^{\dagger}(\vec{r}) \vec{\nabla}^2 [a_{\uparrow}(\vec{r}) a_{\downarrow}(\vec{r})]$.

For $N \geq 7$ we define

$$\delta_{xyz}^2 G_{\psi^2}(t_1, t_2) = L^2 \left\{ G_{\psi^2}(\vec{0}, t_1, t_2) - \frac{1}{6} \left[\begin{array}{l} G_{\psi^2}(\langle 1, 0, 0 \rangle, t_1, t_2) + G_{\psi^2}(\langle -1, 0, 0 \rangle, t_1, t_2) \\ + G_{\psi^2}(\langle 0, 1, 0 \rangle, t_1, t_2) + G_{\psi^2}(\langle 0, -1, 0 \rangle, t_1, t_2) \\ + G_{\psi^2}(\langle 0, 0, 1 \rangle, t_1, t_2) + G_{\psi^2}(\langle 0, 0, -1 \rangle, t_1, t_2) \end{array} \right] \right\}. \quad (65)$$

If no additional ultraviolet renormalization is required, then in the continuum limit we have

$$\delta_x^2 G_{\psi^2}(t_1, t_2) \propto -\partial_x^2 G_{\psi^2}(\vec{0}, t_1, t_2), \quad (66)$$

$$\delta_{xy}^2 G_{\psi^2}(t_1, t_2) \propto -(\partial_x^2 + \partial_y^2) G_{\psi^2}(\vec{0}, t_1, t_2), \quad (67)$$

$$\delta_{xyz}^2 G_{\psi^2}(t_1, t_2) \propto -(\partial_x^2 + \partial_y^2 + \partial_z^2) G_{\psi^2}(\vec{0}, t_1, t_2). \quad (68)$$

To prove that no additional renormalization is needed it suffices to show that one insertion of the operator

$$\frac{1}{\Gamma} a_{\downarrow}^{\dagger}(\vec{r}) a_{\uparrow}^{\dagger}(\vec{r}) \vec{\nabla}^2 [a_{\uparrow}(\vec{r}) a_{\downarrow}(\vec{r})] \quad (69)$$

is finite. Just as we found for the insertion of $a_{\downarrow}^{\dagger}(\vec{r}) a_{\uparrow}^{\dagger}(\vec{r}) a_{\uparrow}(\vec{r}) a_{\downarrow}(\vec{r})$, the factor of Γ^{-1} takes care of the divergences from the two extra fermion bubbles. In the unitary limit the two-particle Green's function has the form

$$G_2(p_0, \vec{p}) \propto \frac{1}{m \sqrt{mp_0 - \frac{\vec{p}^2}{4}}}, \quad (70)$$

where p_0 is the total energy and \vec{p} is the total momentum of the two fermions. Consider now a diagram such as the one shown in FIG. 8. Let p_0 be the energy and \vec{p} be the momentum of the internal loop. We cutoff the momentum at $\Lambda = \pi a^{-1}$ and cutoff the energy at Λ^2/m .

If we now count powers of Λ we get Λ^5 from $dp_0 d^3\vec{p}$, Λ^{-2} from the two Green's functions, Λ^{-6} from the three fermion propagators, and Λ^2 from the $\vec{\nabla}^2$. The final result is Λ^{-1} and so the integral is finite. In this way one can show that all diagrams involving one insertion of

$$\frac{1}{\Gamma} a_{\downarrow}^{\dagger}(\vec{r}) a_{\uparrow}^{\dagger}(\vec{r}) \vec{\nabla}^2 [a_{\uparrow}(\vec{r}) a_{\downarrow}(\vec{r})] \quad (71)$$

are ultraviolet finite. This means that in the unitary limit each of the functions $\delta_x^2 G_{\psi^2}(t_1, t_2)$, $\delta_{xy}^2 G_{\psi^2}(t_1, t_2)$, $\delta_{xyz}^2 G_{\psi^2}(t_1, t_2)$ should be independent of L when considered as functions of $E_F t_1$ and $E_F t_2$.

In FIG. 9 we plot $\ln[\delta_x^2 G_{\psi^2}(t_1, t_2)]$ for the 3, 3 system with $L = 4, 5, 6$. We have produced data for $t_1 = t_2$ and data for t_2 fixed at $E_F t_2 = 1.2$. The agreement for different values of L provides a consistency check of unitary limit scaling. In the continuum language we are calculating the logarithm of $-\partial_x^2 G_{\psi^2}(\vec{0}, t_1, t_2)$. Using the asymptotic expansion (11) we have

$$\begin{aligned} -\partial_x^2 G_{\psi^2}(\vec{0}, t_1, t_2) &= -\partial_x^2 A_{00}(\vec{0}) - \partial_x^2 A_{01}(\vec{0}) e^{-(E_1 - E_0)t_2} \\ &\quad - \partial_x^2 A_{10}(\vec{0}) e^{-(E_1 - E_0)t_1} - \partial_x^2 A_{11}(\vec{0}) e^{-(E_1 - E_0)(t_1 + t_2)} + \dots \end{aligned} \quad (72)$$

The fixed t_2 data as $t_1 \rightarrow \infty$ is useful in extracting $E_1 - E_0$ since the time dependence must be proportional to $e^{-(E_1 - E_0)t_1}$ plus a constant. We see from the plot that $\ln[\delta_x^2 G_{\psi^2}(t_1, t_2)]$ is nearly a straight line for large t_1 . This indicates a small asymptotic value at $t_1 = \infty$, and a nearly pure exponential signal in this time window. We have fitted a straight line to determine the slope of $\ln[\delta_x^2 G_{\psi^2}(t_1, t_2)]$ with respect to $E_F t_1$ for the fixed t_2 data. We do the fit with a common slope for $L = 4, 5, 6$ but possibly different intercepts for the three values of L . While we are only fitting the fixed t_2 data, we see quite clearly the same slope appears in the $t_1 = t_2$ data.

In FIG. 10 we plot $\ln[\delta_{xy}^2 G_{\psi^2}(t_1, t_2)]$ for the 5, 5 system with $L = 4, 5, 6$. We show data for $t_1 = t_2$ and t_2 fixed at $E_F t_2 = 1.6$. We do the same linear fits for the t_2 fixed data in order to extract $E_1 - E_0$. In FIG. 11 we plot $\ln[\delta_{xyz}^2 G_{\psi^2}(t_1, t_2)]$ for the 7, 7 system with $L = 4, 5, 6$. In FIG. 12 we plot $\ln[\delta_{xyz}^2 G_{\psi^2}(t_1, t_2)]$ for the 13, 13 system with $L = 5, 6$.

In all cases we find agreement for different values of L as predicted by unitary limit scaling. In all cases we also find agreement between the slope of the fixed t_2 data and the $t_1 = t_2$ data when plotted as functions of $E_F(t_1 + t_2)$. This implies that the $e^{-(E_1 - E_0)t_1}$ and

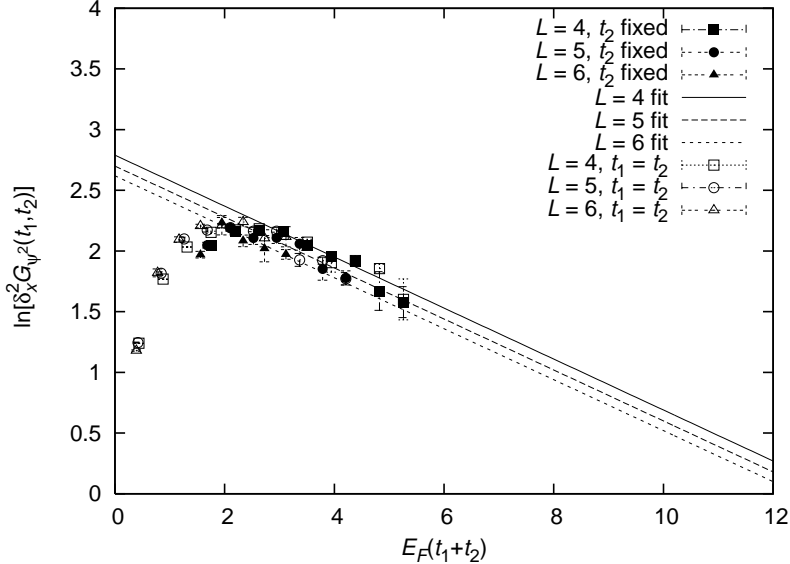


FIG. 9: Plot of $\ln[\delta_x^2 G_{\psi^2}(t_1, t_2)]$ for the 3,3 system with $L = 4, 5, 6$. We show data for $t_1 = t_2$ and t_2 fixed at $E_F t_2 = 1.2$.

$e^{-(E_1 - E_0)t_2}$ terms are small so that

$$-\vec{\nabla}^2 G_{\psi^2}(\vec{0}, t_1, t_2) \approx -\vec{\nabla}^2 A_{00}(\vec{0}) - \vec{\nabla}^2 A_{11}(\vec{0}) e^{-(E_1 - E_0)(t_1 + t_2)}, \quad (73)$$

with $\vec{\nabla}^2$ replaced by ∂_x^2 for the 3,3 system and $\partial_x^2 + \partial_y^2$ for the 5,5 system.

For the moment let us assume that the excitation at energy E_1 can be described as two unknown constituents moving in opposite directions with momentum $\frac{2\pi}{L}$, the minimum nonzero momentum possible on the lattice. This interpretation of the excitation is probably an oversimplification, but it serves as a reasonable starting point to compare with known excitations such as pairs of phonons, quasiparticles, or rotons. In FIG. 13 we plot $(E_1 - E_0)/E_F$ versus momentum k/k_F of the unknown constituents for $N = 3, 5, 7, 9, 11, 13$. For comparison we show the linear part of the two-phonon dispersion relation at unitarity. We use the result [27]

$$c_s = \frac{k_F}{m} \sqrt{\frac{\xi}{3}} \quad (74)$$

for the speed of sound and use the value $\xi = 0.25(3)$ reported in [11]. We see that the minimum in $(E_1 - E_0)/E_F$ at $k \approx 0.8k_F$ falls well below the linear extrapolation for two phonons at $k \approx 0.8k_F$. This appears to rule out a two phonon interpretation.

Since $0.8k_F$ is close to k_F , another reasonable interpretation is that the excitation consists

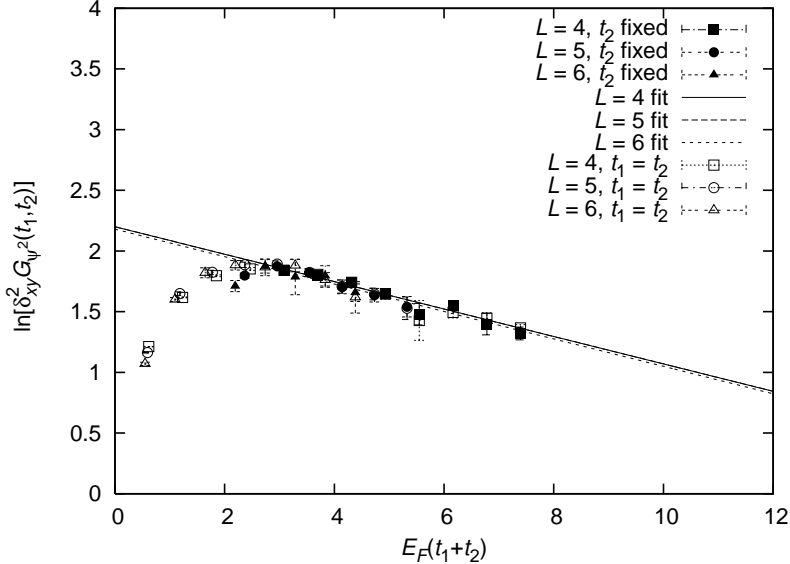


FIG. 10: Plot of $\ln [\delta_{xy}^2 G_{\psi^2}(t_1, t_2)]$ for the 5, 5 system with $L = 4, 5, 6$. We show data for $t_1 = t_2$ and t_2 fixed at $E_F t_2 = 1.6$.

of two fermionic quasiparticles. However here we encounter a similar problem. The energy $E_1 - E_0$ is far below current estimates of 2Δ , where Δ is the even-odd staggering in the ground state energy. Fixed-node Green's function Monte Carlo simulations get a value $\Delta = 0.57(3)E_F$ for 12 – 20 particles in a periodic cube [28] and $\Delta = 0.50(3)E_F$ for 54 – 66 particles [29]. Our own lattice simulations for Δ are in progress, but there is no evidence for Δ being nearly an order of magnitude lower than the fixed-node Monte Carlo results. It could be that the quasiparticles are interacting strongly, but some mechanism would be needed to explain the significant lowering in energy.

A third possibility we consider is that the excitation is a pair of rotons moving in opposite directions. The shape of the dispersion curve in Fig. 13 is similar to the phonon-roton spectrum in superfluid ^4He . Landau [30, 31] first predicted the existence of a roton minimum in superfluid ^4He ,

$$E(k) \approx \Delta_R + \frac{(k - k_R)^2}{2\mu_R}, \quad (75)$$

and Feynman gave a quantum-mechanical description of a roton as an excitation whose wavelength is resonant with the local spatial correlations of identical Bose particles [32, 33, 34]. We briefly summarize the argument below.

Let $\phi_0(\vec{r}_1, \dots, \vec{r}_N)$ be the ground state wavefunction for an interacting system of N

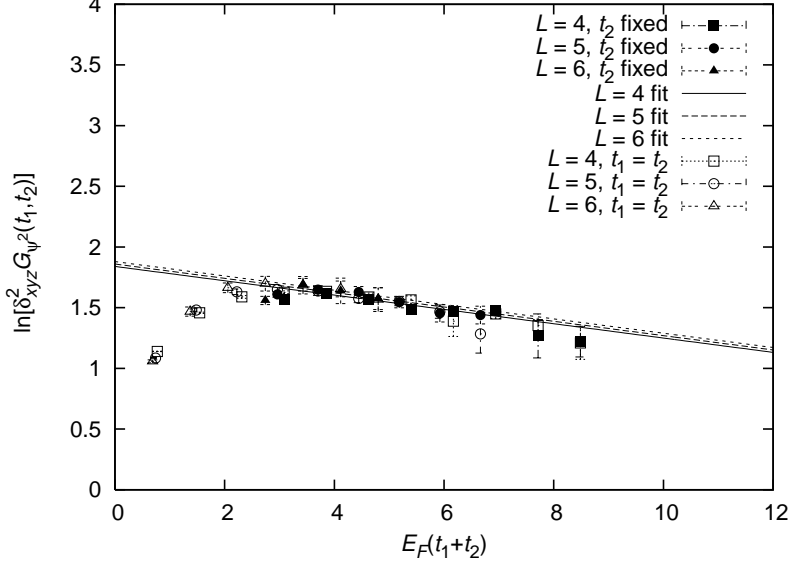


FIG. 11: Plot of $\ln[\delta_{xyz}^2 G_{\psi^2}(t_1, t_2)]$ for the 7,7 system with $L = 4, 5, 6$. We show data for $t_1 = t_2$ and t_2 fixed at $E_F t_2 = 2.0$.

identical bosons with energy E_0 . We construct a trial state $\psi_{\vec{k}}(\vec{r}_1, \dots, \vec{r}_N)$ with momentum \vec{k} defined as

$$\psi_{\vec{k}}(\vec{r}_1, \dots, \vec{r}_N) = \sum_{i=1}^N e^{i\vec{k} \cdot \vec{r}_i} \times \phi_0(\vec{r}_1, \dots, \vec{r}_N). \quad (76)$$

The static structure factor $S(k)$ for the ground state can be written in terms of the square of the norm of $\psi_{\vec{k}}$,

$$\begin{aligned} N \times S(k) &= \int d^{3N} \vec{r} \sum_{l,m=1}^N e^{i\vec{k} \cdot (\vec{r}_l - \vec{r}_m)} \times |\phi_0(\vec{r}_1, \dots, \vec{r}_N)|^2 \\ &= \int d^{3N} \vec{r} |\psi_{\vec{k}}(\vec{r}_1, \dots, \vec{r}_N)|^2 = \langle \psi_{\vec{k}} | \psi_{\vec{k}} \rangle. \end{aligned} \quad (77)$$

Since

$$\begin{aligned} &\langle \psi_{\vec{k}} | H - E_0 | \psi_{\vec{k}} \rangle \\ &= -\frac{1}{2m} \int d^{3N} \vec{r} \sum_{j=1}^N (\vec{\nabla}_j e^{-i\vec{k} \cdot \vec{r}_j})^2 \times |\phi_0(\vec{r}_1, \dots, \vec{r}_N)|^2 = N \frac{k^2}{2m}, \end{aligned} \quad (78)$$

we get

$$\frac{\langle \psi_{\vec{k}} | H - E_0 | \psi_{\vec{k}} \rangle}{\langle \psi_{\vec{k}} | \psi_{\vec{k}} \rangle} = \frac{k^2}{2mS(k)}. \quad (79)$$

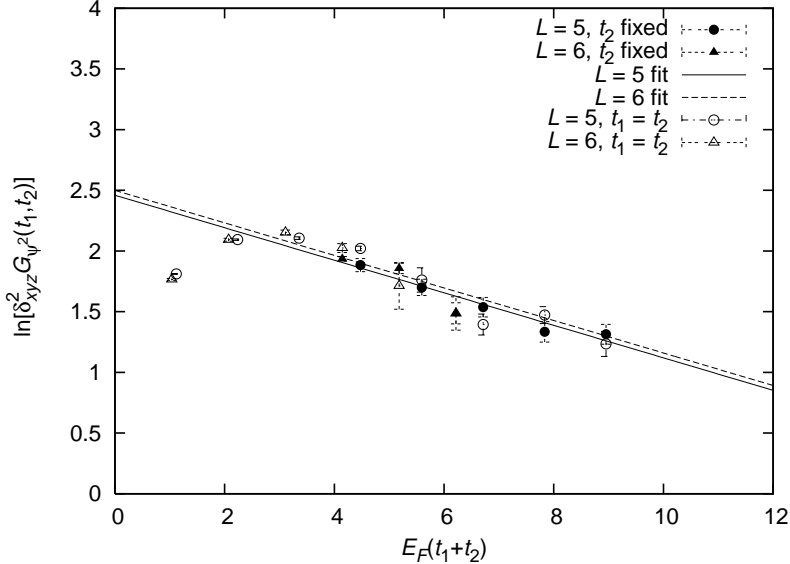


FIG. 12: Plot of $\ln [\delta_{xyz}^2 G_{\psi^2}(t_1, t_2)]$ for the 13,13 system with $L = 5, 6$. We show data for $t_1 = t_2$ and t_2 fixed at $E_F t_2 = 3.0$.

By the variational principle, the energy $E(k)$ for the lowest excitation with momentum \vec{k} satisfies the upper bound

$$E(k) \leq \frac{k^2}{2mS(k)}. \quad (80)$$

This upper bound applies to phonons at small k as well rotons at larger k . For a relatively dense system such as ${}^4\text{He}$ a maximum in $S(k)$ occurs near $k \approx 2\pi/d$, where d is the average spacing between bosons. Therefore a minimum in the upper bound (80) occurs at $k \approx 2\pi/d$, and this may also be reflected in $E(k)$. On the other hand for very dilute Bose systems local spatial correlations are weaker and become significant only at distance scales comparable to the scattering length. In this case the maximum in $S(k)$ has been shown to occur at $k \approx 8/(\pi a_{\text{scatt}})$ [35].

The simple estimate $k_R \approx 2\pi/d$ works rather well for superfluid ${}^4\text{He}$. The particle density of superfluid ${}^4\text{He}$ at $T = 1.25$ K and $P = 1.0$ atm has been measured to be [36]

$$\frac{N}{V} \approx 2.20 \times 10^{-2} \text{\AA}^{-3}. \quad (81)$$

Making a rough estimate for the average spacing

$$d \approx \left(\frac{N}{V} \right)^{-1/3}, \quad (82)$$

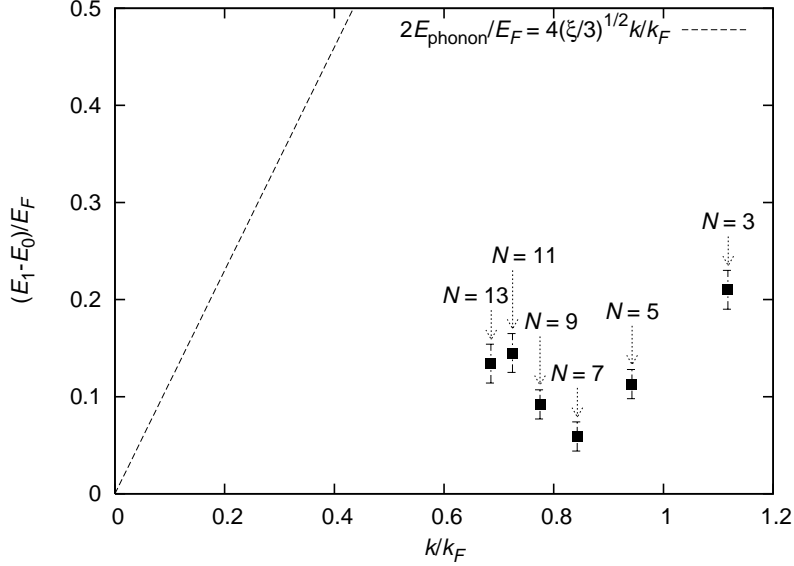


FIG. 13: Plot of $(E_1 - E_0)/E_F$ versus momentum k/k_F of the unknown constituents. For comparison we show the linear part of the two-phonon dispersion relation at unitarity.

we get the prediction

$$k_R^{\text{theory}} \approx \frac{2\pi}{\left(\frac{N}{V}\right)^{-1/3}} = 1.76\text{\AA}^{-1}, \quad (83)$$

which is close to the direct experimental measurement of the roton minimum at $T = 1.26\text{ K}$ and $P = 1.00\text{ atm}$ [37],

$$k_R^{\text{exp}} = 1.902\text{\AA}^{-1}. \quad (84)$$

We return now to our fermionic spin-1/2 system with N up spins and N down spins at unitarity. Let d be the average distance between neighboring pairs of particles. We use the same approximation,

$$d \approx \left(\frac{N}{V}\right)^{-1/3} = N^{-1/3}L, \quad (85)$$

and find that

$$k_R \approx \frac{2\pi}{N^{-1/3}L} = \left(\frac{4\pi}{3}\right)^{1/3} k_F \approx 1.61k_F. \quad (86)$$

Unfortunately this does not describe the minimum of $(E_1 - E_0)/E_F$ at $k \approx 0.8k_F$. In fact the minimum in $(E_1 - E_0)/E_F$ is very close to one-half of k_R . This would appear to rule out the interpretation as two rotons.

It is likely that our systems of 6 – 26 particles have too few particles to get an accurate reading for the excitation spectrum. Indeed there are not enough particles to probe the small k/k_F behavior where the lowest excitations are described by phonons. Perhaps this low-energy excitation changes character and goes up in energy as we include more particles and long wavelength phonons emerge. This is possible. However we should still answer the question of what is happening in the 6 – 26 particle system and how it is able to produce an excitation this low in energy.

XI. TWO-PARTICLE CORRELATIONS

In order to study the properties of the ground state and the unknown excitation in further detail we compute two-particle correlations. For the same N, N system with total momentum $\vec{P} = \vec{0}$ and total spin $S = 0$, we define the opposite-spin two-particle correlation function,

$$\rho_{\downarrow\uparrow}(\vec{r}, t_1, t_2) = \rho_{\uparrow\downarrow}(\vec{r}, t_1, t_2) = \frac{\langle \Psi(t_1) | a_{\uparrow}^{\dagger}(\vec{r}) a_{\uparrow}(\vec{r}) a_{\downarrow}^{\dagger}(\vec{0}) a_{\downarrow}(\vec{0}) | \Psi(t_2) \rangle}{\langle \Psi(t_1) | \Psi(t_2) \rangle}, \quad (87)$$

and the same-spin two-particle correlation function,

$$\rho_{\uparrow\uparrow}(\vec{r}, t_1, t_2) = \rho_{\downarrow\downarrow}(\vec{r}, t_1, t_2) = \frac{\langle \Psi(t_1) | : a_{\downarrow}^{\dagger}(\vec{r}) a_{\downarrow}(\vec{r}) a_{\downarrow}^{\dagger}(\vec{0}) a_{\downarrow}(\vec{0}) : | \Psi(t_2) \rangle}{\langle \Psi(t_1) | \Psi(t_2) \rangle}. \quad (88)$$

In the auxiliary field transfer matrix formalism we compute these correlation functions using

$$\rho_{\uparrow\downarrow}(\vec{n}_s, t_1, t_2) = \frac{\int Ds \langle \Psi(t_1), s | a_{\uparrow}^{\dagger}(\vec{n}_s) a_{\uparrow}(\vec{n}_s) a_{\downarrow}^{\dagger}(\vec{0}) a_{\downarrow}(\vec{0}) | \Psi(t_2), s \rangle \exp \left\{ -\frac{1}{2} \sum_{\vec{n}} [s(\vec{n})]^2 \right\}}{\int Ds \langle \Psi(t_1), s | \Psi(t_2), s \rangle \exp \left\{ -\frac{1}{2} \sum_{\vec{n}} [s(\vec{n})]^2 \right\}}, \quad (89)$$

and

$$\rho_{\downarrow\downarrow}(\vec{n}_s, t_1, t_2) = \frac{\int Ds \langle \Psi(t_1), s | : a_{\downarrow}^{\dagger}(\vec{n}_s) a_{\downarrow}(\vec{n}_s) a_{\downarrow}^{\dagger}(\vec{0}) a_{\downarrow}(\vec{0}) : | \Psi(t_2), s \rangle \exp \left\{ -\frac{1}{2} \sum_{\vec{n}} [s(\vec{n})]^2 \right\}}{\int Ds \langle \Psi(t_1), s | \Psi(t_2), s \rangle \exp \left\{ -\frac{1}{2} \sum_{\vec{n}} [s(\vec{n})]^2 \right\}}. \quad (90)$$

Rather than calculating matrix elements of the two-particle operators in (89) and (90) directly, we define

$$M(\epsilon_{\uparrow}, \epsilon_{\downarrow}, \delta_{\downarrow}) =: \exp \left[\epsilon_{\uparrow} a_{\uparrow}^{\dagger}(\vec{n}_s) a_{\uparrow}(\vec{n}_s) + \epsilon_{\downarrow} a_{\downarrow}^{\dagger}(\vec{n}_s) a_{\downarrow}(\vec{n}_s) + \delta_{\downarrow} a_{\downarrow}^{\dagger}(\vec{0}) a_{\downarrow}(\vec{0}) \right] :. \quad (91)$$

We extract the operators needed for the two-particle correlations by taking derivatives,

$$a_{\uparrow}^{\dagger}(\vec{n}_s)a_{\uparrow}(\vec{n}_s)a_{\downarrow}^{\dagger}(\vec{0})a_{\downarrow}(\vec{0}) = \lim_{\epsilon_{\uparrow}, \epsilon_{\downarrow}, \delta_{\downarrow} \rightarrow 0} \frac{\partial}{\partial \epsilon_{\uparrow}} \frac{\partial}{\partial \delta_{\downarrow}} M(\epsilon_{\uparrow}, \epsilon_{\downarrow}, \delta_{\downarrow}), \quad (92)$$

$$: a_{\downarrow}^{\dagger}(\vec{n}_s)a_{\downarrow}(\vec{n}_s)a_{\downarrow}^{\dagger}(\vec{0})a_{\downarrow}(\vec{0}) := \lim_{\epsilon_{\uparrow}, \epsilon_{\downarrow}, \delta_{\downarrow} \rightarrow 0} \frac{\partial}{\partial \epsilon_{\downarrow}} \frac{\partial}{\partial \delta_{\downarrow}} M(\epsilon_{\uparrow}, \epsilon_{\downarrow}, \delta_{\downarrow}). \quad (93)$$

This construction is useful because $M(\epsilon_{\uparrow}, \epsilon_{\downarrow}, \delta_{\downarrow})$ itself looks like a transfer matrix with only single-nucleon operators.

Let us define the new single-particle matrix elements with one insertion of $M^X(\epsilon_{\uparrow}, \epsilon_{\downarrow}, \delta_{\downarrow})$,

$$M_{ij}(s, t_1, t_2, \epsilon_{\uparrow}, \epsilon_{\downarrow}, \delta_{\downarrow}) = \langle p_i^X | M_{n_{t_1} + n_{t_2} - 1}^X(s) \times \cdots \times M_{n_{t_2}}^X(s) M^X(\epsilon_{\uparrow}, \epsilon_{\downarrow}, \delta_{\downarrow}) M_{n_{t_2} - 1}^X(s) \times \cdots \times M_0^X(s) | p_j^X \rangle, \quad (94)$$

We let

$$\rho(t_1, t_2, \epsilon_{\uparrow}, \epsilon_{\downarrow}, \delta_{\downarrow}) = \frac{\int Ds \exp \left\{ -\frac{1}{2} \sum_{\vec{n}} [s(\vec{n})]^2 \right\} \det M(s, t_1, t_2, \epsilon_{\uparrow}, \epsilon_{\downarrow}, \delta_{\downarrow})}{\int Ds \exp \left\{ -\frac{1}{2} \sum_{\vec{n}} [s(\vec{n})]^2 \right\} \det M(s, t_1 + t_2)}. \quad (95)$$

Then

$$\rho_{\uparrow\downarrow}(\vec{n}_s, t_1, t_2) = \lim_{\epsilon_{\uparrow}, \epsilon_{\downarrow}, \delta_{\downarrow} \rightarrow 0} \frac{\partial}{\partial \epsilon_{\uparrow}} \frac{\partial}{\partial \delta_{\downarrow}} \rho(t_1, t_2, \epsilon_{\uparrow}, \epsilon_{\downarrow}, \delta_{\downarrow}). \quad (96)$$

$$\rho_{\downarrow\downarrow}(\vec{n}_s, t_1, t_2) = \lim_{\epsilon_{\uparrow}, \epsilon_{\downarrow}, \delta_{\downarrow} \rightarrow 0} \frac{\partial}{\partial \epsilon_{\downarrow}} \frac{\partial}{\partial \delta_{\downarrow}} \rho(t_1, t_2, \epsilon_{\uparrow}, \epsilon_{\downarrow}, \delta_{\downarrow}), \quad (97)$$

XII. RESULTS FOR $\rho_{\uparrow\downarrow}$ AND $\rho_{\downarrow\downarrow}$

We compute $\rho_{\uparrow\downarrow}(\vec{n}_s, t/2, t/2)$ and $\rho_{\downarrow\downarrow}(\vec{n}_s, t/2, t/2)$ for $N = 5$ and $L = 4$ using the same initial state $|\Psi_0^{\text{free}}\rangle$ used previously to calculate $G_{\psi^2}^{\text{bare}}(\vec{n}_s, t/2, t/2)$. We recall that our initial state for $N = 5$ corresponds with single particle momenta $\langle 0, 0, 0 \rangle$, $\langle \frac{2\pi}{L}, 0, 0 \rangle$, $\langle -\frac{2\pi}{L}, 0, 0 \rangle$, $\langle 0, \frac{2\pi}{L}, 0 \rangle$, and $\langle 0, -\frac{2\pi}{L}, 0 \rangle$. For each lattice calculation we have performed several consistency checks for $\rho_{\uparrow\downarrow}(\vec{n}_s, t/2, t/2)$ and $\rho_{\downarrow\downarrow}(\vec{n}_s, t/2, t/2)$. Summing $\rho_{\uparrow\downarrow}(\vec{n}_s, t/2, t/2)$ over \vec{n}_s and multiplying by L^3 counts the number of ways to select two particles with opposite spins,

$$L^3 \sum_{\vec{n}_s} \rho_{\uparrow\downarrow}(\vec{n}_s, t_1, t_2) = N^2. \quad (98)$$

The same procedure for $\rho_{\downarrow\downarrow}(\vec{n}_s, t/2, t/2)$ counts the number of ways to select two down-spin particles without replacement,

$$L^3 \sum_{\vec{n}_s} \rho_{\downarrow\downarrow}(\vec{n}_s, t/2, t/2) = N(N - 1). \quad (99)$$

One last consistency check uses the fact that

$$a_{\uparrow}^{\dagger}(\vec{0})a_{\uparrow}(\vec{0})a_{\downarrow}^{\dagger}(\vec{0})a_{\downarrow}(\vec{0}) = a_{\downarrow}^{\dagger}(\vec{0})a_{\downarrow}(\vec{0})a_{\uparrow}^{\dagger}(\vec{0})a_{\uparrow}(\vec{0}). \quad (100)$$

From this we deduce that

$$\rho_{\uparrow\downarrow}(\vec{0}, t/2, t/2) = G_{\psi^2}^{\text{bare}}(\vec{0}, t/2, t/2). \quad (101)$$

The results of the three consistency checks are shown in Table 6. We see that all ratios are in agreement with the required value of 1.

$E_F t$	$\frac{L^3}{N^2} \sum_{\vec{n}_s} \rho_{\uparrow\downarrow}(\vec{n}_s, t/2, t/2)$	$\frac{L^3}{N(N-1)} \sum_{\vec{n}_s} \rho_{\downarrow\downarrow}(\vec{n}_s, t/2, t/2)$	$\frac{\rho_{\uparrow\downarrow}(\vec{0}, t/2, t/2)}{G_{\psi^2}^{\text{bare}}(\vec{0}, t/2, t/2)}$
0	1.00	1.00	1.00
1.23	1.00(1)	1.00(1)	1.00(2)
2.46	1.00(1)	1.00(1)	1.01(1)
3.70	1.00(1)	1.00(1)	1.01(1)
4.93	0.99(1)	0.99(1)	0.99(2)
6.16	1.01(1)	1.01(1)	1.02(1)
7.39	0.98(2)	0.98(2)	0.98(3)

Table 6: Consistency checks for $\rho_{\uparrow\downarrow}$ and $\rho_{\downarrow\downarrow}$. Each entry should equal 1.

We show results for $G_{\psi^2}^{\text{bare}}(\vec{n}_s, t/2, t/2)$, $\rho_{\uparrow\downarrow}(\vec{n}_s, t/2, t/2)$, and $\rho_{\downarrow\downarrow}(\vec{n}_s, t/2, t/2)$ with \vec{n}_s in the xy -plane in FIG. 14. The same results for \vec{n}_s in the xz -plane are shown FIG. 15. In our contour plots the maximum brightness for $G_{\psi^2}^{\text{bare}}$ corresponds with 0.05, while the maximum brightness for $\rho_{\uparrow\downarrow}$ and $\rho_{\downarrow\downarrow}$ corresponds with 0.01. For $N = 5$ the ground state of the free Fermi system is degenerate. We have chosen the initial state $|\Psi_0^{\text{free}}\rangle$ with all momenta orthogonal to the z -direction. This explains the lack of cubic $SO(3, \mathbb{Z})$ invariance in the xz -plane data, especially for smaller values of $E_F t$. At the largest value $E_F t = 7.39$ the xz -plane data shows signs of cubic rotational invariance and is beginning to resemble the xy -plane data at $E_F t = 7.39$.

We see that already for $E_F t \geq 1.23$ a sharp maximum in $\rho_{\uparrow\downarrow}$ appears at $\vec{n}_s = 0$. This indicates significant spatial correlation between up-spin and down-spin particles due to the strong zero-range attractive force. Another indication of this spatial correlation is that for larger values of $E_F t$ and \vec{n}_s away from the origin, the shape and strength of $\rho_{\uparrow\downarrow}$ and $\rho_{\downarrow\downarrow}$ are nearly identical. Another visible pattern is that regions of maximum strength for $G_{\psi^2}^{\text{bare}}$

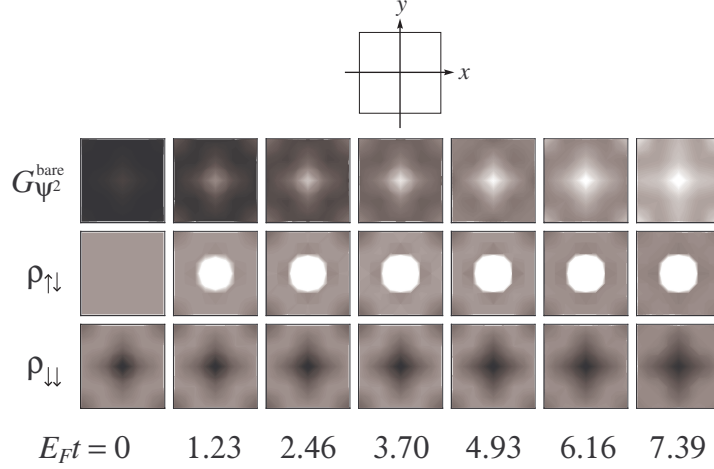


FIG. 14: $G_{\psi^2}^{\text{bare}}(\vec{n}_s, t/2, t/2)$, $\rho_{\uparrow\downarrow}(\vec{n}_s, t/2, t/2)$, $\rho_{\downarrow\downarrow}(\vec{n}_s, t/2, t/2)$ with \vec{n}_s in the xy -plane for $N = 5$ and $L = 4$.

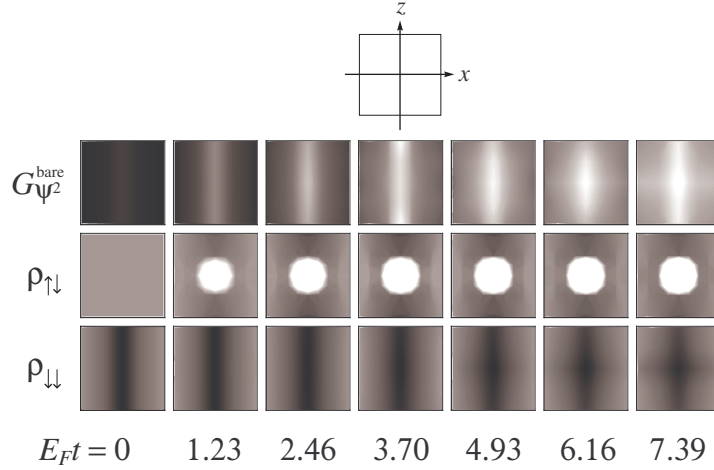


FIG. 15: $G_{\psi^2}^{\text{bare}}(\vec{n}_s, t/2, t/2)$, $\rho_{\uparrow\downarrow}(\vec{n}_s, t/2, t/2)$, $\rho_{\downarrow\downarrow}(\vec{n}_s, t/2, t/2)$ with \vec{n}_s in the xz -plane for $N = 5$ and $L = 4$.

correlate with regions of minimum strength for $\rho_{\downarrow\downarrow}$. Conversely the minima for $G_{\psi^2}^{\text{bare}}$ are maxima in $\rho_{\downarrow\downarrow}$. This is most likely the direct result of Pauli blocking.

The crosslike pattern that emerges in $G_{\psi^2}^{\text{bare}}$ and $\rho_{\downarrow\downarrow}$ is the same $2\pi/L$ cosine wave excitation we have been investigating. We note that the same pattern can be reproduced rather simply with two up-spin and two down-spin particles. Let $|\Psi_x\rangle$ be the normalized four

particle state,

$$|\Psi_x\rangle = \frac{1}{L^6\sqrt{2}} \left[\tilde{a}_\uparrow^\dagger(-\vec{p}_x)\tilde{a}_\downarrow^\dagger(\vec{p}_x) + \tilde{a}_\uparrow^\dagger(\vec{p}_x)\tilde{a}_\downarrow^\dagger(-\vec{p}_x) \right] \tilde{a}_\uparrow^\dagger(\vec{0})\tilde{a}_\downarrow^\dagger(\vec{0}) |0\rangle, \quad (102)$$

$$\vec{p}_x = \left\langle \frac{2\pi}{L}, 0, 0 \right\rangle. \quad (103)$$

Similarly let $|\Psi_z\rangle$ be

$$|\Psi_z\rangle = \frac{1}{L^6\sqrt{2}} \left[\tilde{a}_\uparrow^\dagger(-\vec{p}_z)\tilde{a}_\downarrow^\dagger(\vec{p}_z) + \tilde{a}_\uparrow^\dagger(\vec{p}_z)\tilde{a}_\downarrow^\dagger(-\vec{p}_z) \right] \tilde{a}_\uparrow^\dagger(\vec{0})\tilde{a}_\downarrow^\dagger(\vec{0}) |0\rangle, \quad (104)$$

$$\vec{p}_z = \left\langle 0, 0, \frac{2\pi}{L} \right\rangle. \quad (105)$$

We define t -independent expressions $G_{\psi^2}^{\text{bare}}(\vec{n}_s, \Psi_{x,z})$ and $\rho_{\downarrow\downarrow}(\vec{n}_s, \Psi_{x,z})$ for the states $|\Psi_x\rangle$ and $|\Psi_z\rangle$,

$$G_{\psi^2}^{\text{bare}}(\vec{n}_s, \Psi_{x,z}) = \langle \Psi_{x,z} | a_\downarrow^\dagger(\vec{n}_s) a_\uparrow(\vec{n}_s) a_\uparrow^\dagger(\vec{0}) a_\downarrow(\vec{0}) | \Psi_{x,z} \rangle \quad (106)$$

$$\rho_{\downarrow\downarrow}(\vec{n}_s, \Psi_{x,z}) = \langle \Psi_{x,z} | : a_\downarrow^\dagger(\vec{n}_s) a_\downarrow(\vec{n}_s) a_\downarrow^\dagger(\vec{0}) a_\downarrow(\vec{0}) : | \Psi_{x,z} \rangle. \quad (107)$$

The first column in FIG. 16 shows $G_{\psi^2}^{\text{bare}}$ and $\rho_{\downarrow\downarrow}$ for $|\Psi_x\rangle$. The second column shows $G_{\psi^2}^{\text{bare}}$ and $\rho_{\downarrow\downarrow}$ averaged for $|\Psi_x\rangle$ and $|\Psi_z\rangle$. The third column shows the same data as the second column but cropped to a region of size $d \times d$, where $d \approx N^{-1/3}L$ is the average spacing between particles. For these contour plots the maximum brightness for $G_{\psi^2}^{\text{bare}}$ corresponds with 0.00125, while the maximum brightness for $\rho_{\downarrow\downarrow}$ corresponds with 0.001. We note that the intensity scale for $\rho_{\downarrow\downarrow}$ is a factor of ten lower than that in FIGS. 14 and 15. This is consistent with the sum rule in (99) since we have reduced $N(N-1)$ from 20 to 2. The ratio of intensities between $G_{\psi^2}^{\text{bare}}$ and $\rho_{\downarrow\downarrow}$ in FIGS. 14 and 15 is a factor of four larger than that in FIG. 16. This implies that the actual excitation has stronger spatial correlations between up and down spins than our simple plane-wave states $|\Psi_x\rangle$ and $|\Psi_z\rangle$.

We find that the $d \times d$ region in the third column of (16) describes the transient signal in $G_{\psi^2}^{\text{bare}}$ and $\rho_{\downarrow\downarrow}$ for large $E_F t$. In fact this holds true for all systems we have checked, $N = 3, 5, 7, 9, 11, 13$. This would suggest that the excitation is some type of quasi-1D system of four particles wrapped around the periodic lattice. The $d \times d$ window would suggest a transverse width of approximately d for the quasi-1D system. Outside the $d \times d$ region it is more difficult to discern a universal pattern in the data for all N .

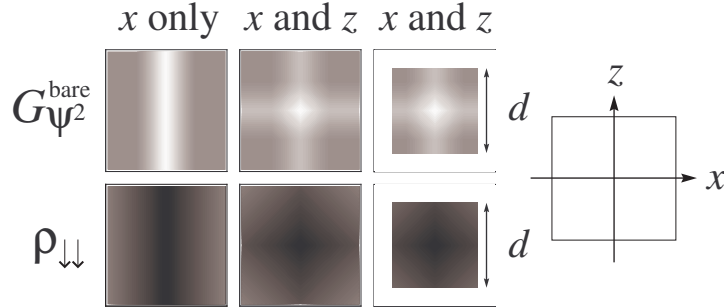


FIG. 16: The first column shows $G_{\psi^2}^{\text{bare}}$ and $\rho_{\downarrow\downarrow}$ for $|\Psi_x\rangle$. The second column shows $G_{\psi^2}^{\text{bare}}$ and $\rho_{\downarrow\downarrow}$ averaged for $|\Psi_x\rangle$ and $|\Psi_z\rangle$. The third column shows the same data as the second column but cropped to a region of size $d \times d$.

XIII. SUMMARY AND DISCUSSION

We have presented lattice results for spin-1/2 fermions at unitarity, where the effective range of the interaction is zero and the scattering length is infinite. We measured the spatial coherence of difermion pairs for a system of particles with equal numbers of up and down spins in a periodic cube. Using a transfer matrix projection method with auxiliary fields, we analyzed both ground state properties and transient behavior due to low-energy excitations. We first measured Γ , the probability that a given lattice site has both an up-spin and down-spin particle. From this we were able to deduce that $\xi_1 = 1.0(1)$, where ξ_1 is defined by

$$\frac{E_0}{N + N} = \frac{3}{5} \frac{k_F^2}{2m} [\xi - \xi_1 k_F^{-1} a_{\text{scatt}}^{-1} + O(k_F^{-2} a_{\text{scatt}}^{-2})]. \quad (108)$$

We then measured the pair correlation function at nonzero spatial separation and found clear evidence of off-diagonal long-range order. This suggests that the ground state is superfluid with s-wave pairing.

We also found evidence for a low-energy excitation with energy E_1 which ranges between $0.05E_F$ and $0.2E_F$ for $N = 3, 5, 7, 9, 11, 13$. We note that recent radio frequency measurements of the excitation spectra in ${}^6\text{Li}$ at unitarity has found an energy gap in the unpolarized system at roughly $0.2E_F$ [38]. The low value for the excitation energy would tend to drive down the superfluid critical temperature and create a pseudogap phase where single fermionic quasiparticles are gapped at Δ while the new excitation is gapped at a lower

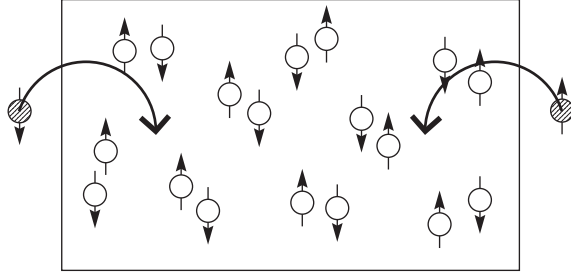


FIG. 17: Starting with the ground state, we insert one extra up-spin and one extra down-spin.

energy scale. An estimate of the effect on the critical temperature requires a better understanding of the energy gap in large systems, the density of states, and possible interactions. It is possible though that this excitation could explain the consistently low critical temperature measured in recent lattice simulations which have specifically looked for off-diagonal long-range order [17, 20, 39, 40].

The low-energy excitation corresponding with E_1 in systems $N = 3, 5, 7, 9, 11, 13$ appears to be inconsistent with an interpretation as a pair of weakly interacting phonons, fermionic quasiparticles, or rotons. By examining the pair correlation function as well as two-particle density correlations, we find the excitation has the characteristics of a quasi-1D chain consisting of two up-spin and two down-spin particles aligned along one of the lattice axes. We caution that this excitation could be an artifact due to the periodic boundary with a relatively small number of particles. Confirmation in lattice systems with more particles and different geometries will be needed. The exact mechanism which produces the quasi-1D chain is beyond the scope of this study. However we can present here at least one plausible explanation.

Consider the ground state of the unitary limit system with $N - 1$ up spins and $N - 1$ down spins. Let d be the average separation between particles. We now introduce one extra up-spin and one extra down-spin separated by a distance $x > d$ as shown in FIG. 17. Next we evolve the state forward in Euclidean time using the projection operator e^{-Ht} . If $x \gg \sqrt{t/m} \sim d$ then the projection time is not sufficient to find the true ground state of the N, N system. Instead we have two essentially non-interacting quasiparticles, and the expectation value of the energy after Euclidean time t will be roughly 2Δ above the ground state energy, where Δ is the even-odd pairing gap.

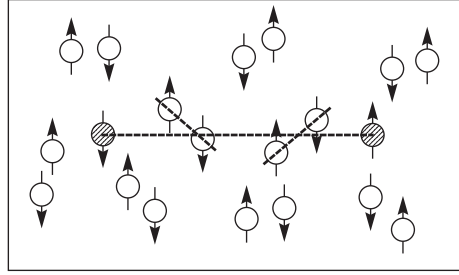


FIG. 18: The pairs located near a line segment connecting the extra particles favor an orientation with the up spins to the left and down spins to the right.

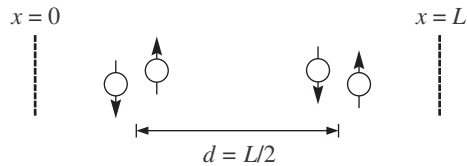


FIG. 19: Two up spins and two down spins aligned along one of the lattice axes.

If however $x \gtrsim \sqrt{t/m} \sim d$, then pairs nearby the extra particles may rearrange themselves slightly to lower the total energy as shown in FIG. 18. Pairs located near a line segment connecting the extra particles favor an orientation with up spins to the left and down spins to the right. The tilt angle with respect to the line segment may prefer to alternate from one pair to the next. The resulting state could be described as a pair of quasiparticles interacting via a loose chain of pairs connecting them. The transverse width of this chain would be roughly equal to d .

Chain configurations without specified endpoints can also be constructed. In FIG. 19 we show a four-particle chain extending across the periodic lattice. From the symmetry of the four-particle chain configuration we expect the resonance energy to be minimized when the average spacing between particles equals $L/2$. Using a simple estimate for the average separation, $d \approx L/N^{1/3}$, we find that a minimum in energy should occur at $N \approx 8$. This is consistent with the N -dependence of $(E_1 - E_0)/E_F$ shown in FIG. 13. Further studies will be needed to see if longer quasi-1D chains exist and if excitations can be found which do not wind around the periodic lattice. If longer chains are possible then we might expect resonances in a periodic cube for $d = L/j$ for each integer $j \geq 2$. This corresponds with

$N \approx j^3$. However the alternation of tilt angle between neighboring pairs will be frustrated for odd j

In our discussion we have tried to put an emphasis on universal observables in the unitary limit. These are observables which agree in different physical systems at unitarity, such as critical temperature, critical velocity, speed of sound, low-energy excitation energies, etc. The reason for the emphasis on universal observables is that different microscopic theories can agree on all low-energy physical observables but disagree on wavefunctions and off-shell Green's functions. In order to make contact with recent observations of superfluidity with trapped ultracold atoms [38, 41, 42, 43, 44, 45], it seems important for both theory and experiment to identify truly universal properties of the unitary limit. There has been some recent work on the non-universality of fermion momentum occupation numbers with respect to field redefinitions [46, 47]. By analogy similar issues have been raised concerning the universality of superfluid condensate fractions for a low-energy effective theory without specification of the fundamental microscopic physics.

XIV. ACKNOWLEDGEMENTS

The author is grateful to Gautam Rupak and Thomas Schäfer for many stimulating discussions. This work is supported in part by the DOE grant DE-FG02-04ER41335.

-
- [1] D. M. Eagles, Phys. Rev. **186**, 456 (1969).
 - [2] A. J. Leggett, in *Modern Trends in the Theory of Condensed Matter. Proceedings of the XVIth Karpacz Winter School of Theoretical Physics, Karpacz, Poland, 1980* (Springer-Verlag, Berlin, 1980), p. 13.
 - [3] P. Nozieres and S. Schmitt-Rink, J. Low Temp. Phys. **59**, 195 (1985).
 - [4] Q. Chen, J. Stajic, S. Tan, and K. Levin, Physics Reports **412**, 1 (2005).
 - [5] E. Tiesinga, B. J. Verhaar, and H. T. C. Stoof, Phys. Rev. **A47**, 4114 (1993).
 - [6] W. C. Stwalley, Phys. Rev. Lett. **37**, 1628 (1976).
 - [7] P. Courteille, R. S. Freeland, D. J. Heinzen, F. A. van Abeelen, and B. J. Verhaar, Phys. Rev. Lett. **81**, 69 (1998).

- [8] S. Inouye, M. R. Andrews, J. Stenger, H.-J. Miesner, D. Stamper-Kurn, and W. Ketterle, *Nature* **392**, 151 (1998).
- [9] C. J. Pethick and D. G. Ravenhall, *Ann. Rev. Nucl. Part. Sci.* **45**, 429 (1995).
- [10] J. M. Lattimer and M. Prakash (2004), astro-ph/0405262.
- [11] D. Lee, *Phys. Rev.* **B73**, 115112 (2006), cond-mat/0511332.
- [12] O. Penrose and L. Onsager, *Phys. Rev.* **104**, 576 (1956).
- [13] L. P. Gor'kov, *Soviet Phys. JETP* **7**, 505 (1958).
- [14] J.-W. Chen and D. B. Kaplan, *Phys. Rev. Lett.* **92**, 257002 (2004), hep-lat/0308016.
- [15] D. Lee and T. Schaefer, *Phys. Rev.* **C72**, 024006 (2005), nucl-th/0412002.
- [16] D. Lee, B. Borasoy, and T. Schaefer, *Phys. Rev.* **C70**, 014007 (2004), nucl-th/0402072.
- [17] M. Wingate (2005), cond-mat/0502372.
- [18] A. Bulgac, J. E. Drut, and P. Magierski, *Phys. Rev. Lett.* **96**, 090404 (2006), cond-mat/0505374.
- [19] D. Lee and T. Schafer, *Phys. Rev.* **C73**, 015201 (2006), nucl-th/0509017.
- [20] D. Lee and T. Schafer, *Phys. Rev.* **C73**, 015202 (2006), nucl-th/0509018.
- [21] M. Creutz, *Phys. Rev.* **D38**, 1228 (1988).
- [22] M. Creutz, *Found. Phys.* **30**, 487 (2000), hep-lat/9905024.
- [23] B. Borasoy, H. Krebs, D. Lee, and U.-G. Meißner, *Nucl. Phys.* **A768**, 179 (2006), nucl-th/0510047.
- [24] M. Lüscher, *Commun. Math. Phys.* **105**, 153 (1986).
- [25] S. R. Beane, P. F. Bedaque, A. Parreno, and M. J. Savage, *Phys. Lett.* **B585**, 106 (2004), hep-lat/0312004.
- [26] S. Duane, A. D. Kennedy, B. J. Pendleton, and D. Roweth, *Phys. Lett.* **B195**, 216 (1987).
- [27] D. T. Son and M. Wingate, *Annals Phys.* **321**, 197 (2006), cond-mat/0509786.
- [28] S. Y. Chang, V. R. Pandharipande, J. Carlson, and K. E. Schmidt, *Phys. Rev.* **A70**, 043602 (2004).
- [29] J. Carlson and S. Reddy, *Phys. Rev. Lett.* **95**, 060401 (2005), cond-mat/0503256.
- [30] L. D. Landau, *J. Phys.* **5**, 71 (1941).
- [31] L. D. Landau, *J. Phys.* **11**, 91 (1947).
- [32] R. P. Feynman, *Phys. Rev.* **91**, 1301 (1953).
- [33] R. P. Feynman, *Phys. Rev.* **94**, 262 (1954).

- [34] R. P. Feynman and M. Cohen, Phys. Rev. **102**, 1189 (1956).
- [35] J. Steinhauer, R. Ozeri, N. Katz, and N. Davidson (2003), cond-mat/0303375.
- [36] W. H. Keesom, *Helium* (Elsevier, Amsterdam, 1942).
- [37] O. W. Dietrich, E. H. Graf, C. H. Huang, and L. Passell, Phys. Rev. **A5**, 1377 (1972).
- [38] C. Chin, M. Bartenstein, A. Altmeyer, S. Riedl, S. Jochim, J. Hecker Denschlag, and R. Grimm, Science **305**, 1128 (2004), cond-mat/0405632.
- [39] E. Burovski, N. Prokofev, B. Svistunov, and M. Troyer, Phys. Rev. Lett. **96**, 160402 (2006), cond-mat/0602224.
- [40] E. Burovski, N. Prokofev, B. Svistunov, and M. Troyer, New J. Phys. **8**, 153 (2006), cond-mat/0605350.
- [41] C. A. Regal, M. Greiner, and D. S. Jin, Phys. Rev. Lett. **92**, 040403 (2004).
- [42] J. Kinast, S. L. Hemmer, M. E. Gehm, A. Turlapov, and J. E. Thomas, Phys. Rev. Lett. **92**, 150402 (2004).
- [43] M. W. Zwierlein, C. A. Stan, C. H. Schunck, S. M. F. Raupach, A. J. Kerman, and W. Ketterle, Phys. Rev. Lett. **92**, 120403 (2004), cond-mat/0403049.
- [44] M. Bartenstein, A. Altmeyer, S. Riedl, S. Jochim, C. Chin, J. Hecker Denschlag, and R. Grimm, Phys. Rev. Lett. **92**, 120401 (2004).
- [45] M. W. Zwierlein, J. R. Abo-Shaeer, A. Schirotzek, C. H. Schunck, and W. Ketterle, Nature **435**, 1047 (2005), cond-mat/0505635.
- [46] R. J. Furnstahl, H.-W. Hammer, and N. Tirfessa, Nucl. Phys. **A689**, 846 (2001), nucl-th/0010078.
- [47] R. J. Furnstahl and H. W. Hammer, Phys. Lett. **B531**, 203 (2002), nucl-th/0108069.